Molecular Pharmacology Fast Forward. Published on May 1, 2019 as DOI: 10.1124/mol.118.114801
This article has not been copyedited and formatted. The final version may differ from this version.

MOL#114801

Colchicine binding site agent DJ95 overcomes drug resistance and exhibits antitumor efficacy

Authors: Kinsie E. Arnst[1], Yuxi Wang[2,3], Zi-Ning Lei[4], Dong-Jin Hwang[1], Gyanendra Kumar[5], Dejian Ma[1], Deanna N. Parke[6], Qiang Chen[2], Jinliang Yang[2], Stephen W. White[5], Tiffany N. Seagroves[6], Zhe-Sheng Chen[4], Duane D. Miller*[1], and Wei Li*[1]

Affiliation: [1]Department of Pharmaceutical Sciences, College of Pharmacy, the University of Tennessee Health Science Center, Memphis, TN. [2]State Key Laboratory of Biotherapy and Cancer Center, Collaborative Innovation Center of Biotherapy, [3] Department of Respiratory Medicine, West China Hospital, Sichuan University, Chengdu, China. [4]Department of Pharmaceutical Sciences, College of Pharmacy and Health Sciences, St. John's University, Queens, NY. [5] Department of Structural Biology, St. Jude Children's Research Hospital, Memphis, TN. [6]Department of Pathology, the University of Tennessee Health Science Center, Memphis, TN

Molecular Pharmacology Fast Forward. Published on May 1, 2019 as DOI: 10.1124/mol.118.114801
This article has not been copyedited and formatted. The final version may differ from this version.

RUNNING TITLE PAGE

Tubulin inhibitor DJ95 overcomes drug resistance in cancer

Corresponding author:

Wei Li, Ph.D., Address: 881 Madison Avenue, room 561, Memphis, TN 38163. Phone: 901-448-7532, Email: wli@uthsc.edu

Duane D. Miller, Ph.D., Address: 881 Madison Avenue, room 564, Memphis, TN 38163. Phone: 901-448-6027, Email: dmiller@uthsc.edu

Text pages: 30

Tables: 4

Figures: 8

References: 89

Abstract: 241

Introduction: 684

Discussion: 1152

List of nonstandard abbreviations

ABC, ATP-binding cassette;

ANOVA, analysis of variance;

AUC, area under the curve;

BCRP, breast cancer resistant protein

COSMIC, Catalogue of Somatic Mutations in Cancer;

DMSO, dimethyl sulfoxide;

Molecular Pharmacology Fast Forward. Published on May 1, 2019 as DOI: 10.1124/mol.118.114801
This article has not been copyedited and formatted. The final version may differ from this version.

FBS, fetal bovine serum;

GPCR, G-coupled protein receptor;

HUVEC, human umbilical vein endothelial cells;

i.p., intraperitoneal;

MDR, multidrug resistance;

MDR1, multidrug resistant protein 1

MRP1; multidrug resistant-associated protein 1;

MTD, maximum tolerable dose;

NCI/DTP, National Cancer Institute Developmental Therapeutics Program;

PBS, phosphate buffered saline;

PEG, polyethylene glycol;

P-gp, P-glycoprotein;

RI, resistant index;

TGI Tumor growth inhibition, total growth inhibition;

T2R-TTL, Tubulin-RB3_SLD-TTL;

TTL, tubulin tyrosine ligase;

TxR, taxane-resistant;

VDA, vascular disrupting agent

Molecular Pharmacology Fast Forward. Published on May 1, 2019 as DOI: 10.1124/mol.118.114801
This article has not been copyedited and formatted. The final version may differ from this version.

ABSTRACT

Interfering with microtubule dynamics is a well-established strategy for cancer treatment, but many microtubule targeting agents are associated with drug resistance and adverse effects. Substantial evidence points to ATP-binding cassette transporters as critical players in the development of resistance. Herein, we demonstrate the efficacy of DJ95, a novel tubulin inhibitor, in a variety of cancer cell lines, including malignant melanomas, drug selected resistant cell lines, specific ABC transporter over-expressing cell lines, and in the NCI-60 cell line panel. DJ95 treatment inhibited cancer cell migration, caused morphological changes to the microtubule network foundation, and severely disrupted mitotic spindle formation of mitotic cells. The high-resolution crystal structure of DJ95 in complex with tubulin protein and the detailed molecular interactions confirmed its direct binding to the colchicine site. In vitro pharmacological screening of DJ95 using SafetyScreen44 revealed no significant off-target interactions, and pharmacokinetic analysis showed that DJ95 was maintained at therapeutically relevant plasma concentrations for up to 24 hours in ICR mice. In an A375 xenograft model in nude mice, DJ95 inhibited tumor growth and disrupted tumor vasculature in xenograft tumors. These results demonstrate that DJ95 is potent against a variety of cell lines, demonstrated greater potency to ABC transporters over-expressing cell lines than existing tubulin inhibitors, directly targets the colchicine binding domain, exhibits significant anti-tumor efficacy, and demonstrates vascular-disrupting properties. Collectively, these data suggest that DJ95 has great potential as a cancer therapeutic, particularly for multidrug resistance phenotypes, and warrants further development.

Molecular Pharmacology Fast Forward. Published on May 1, 2019 as DOI: 10.1124/mol.118.114801
This article has not been copyedited and formatted. The final version may differ from this version.

INTRODUCTION

Microtubules are cytoskeletal structures that are essential for a variety of cellular events including movement, intracellular transport, cell signaling, and mitosis (Jordan, 2002; Kavallaris, 2010; Pasquier and Kavallaris, 2008; Perez, 2009b). Microtubules are composed of α- and β-tubulin proteins, which readily undergo polymerization and depolymerization in a phenomenon known as dynamic instability (Mitchison and Kirschner, 1984). They also form the highly dynamic mitotic spindles that are responsible for the alignment and segregation of chromosomes in the cell during mitosis (Kline-Smith and Walczak, 2004). Interference with microtubule dynamics consequently disrupts mitotic progression and ultimately leads to apoptosis and cell death (Schmidt and Bastians, 2007). Therefore, interfering with microtubule dynamics by targeting tubulin with small molecules is a validated anticancer strategy, and many agents are already used clinically or are undergoing development (Dorleans et al., 2009; Gigant et al., 2005; Perez, 2009b; Ravelli et al., 2004).

Tubulin inhibitors can be broadly divided into two categories: microtubule stabilizing agents (e.g. taxanes) or destabilizing agents (e.g. vinca alkaloids, colchicine binding site agents). Currently, all approved tubulin inhibitors for cancer therapy target the taxane or vinca alkaloid binding site. However, many tubulin inhibitors, including paclitaxel (Taxol®), are associated with multidrug resistance (MDR) mechanisms such as overexpression of drug efflux pumps or the βIII tubulin isoform (Kamath et al., 2005; Lu et al., 2012; Morris and Fornier, 2008; Orr et al., 2003). Drug efflux mediated by ATP-binding cassette (ABC) transporters is the most commonly observed mechanism responsible for inhibiting the intracellular accumulation of therapeutic agents in resistant cell lines(Szakacs et al., 2006). Of the known human ABC transporters, resistant melanoma cells have been shown to overexpress ABCB1 (MDR1, P-gp), ABCC1 (MRP1),

Molecular Pharmacology Fast Forward. Published on May 1, 2019 as DOI: 10.1124/mol.118.114801
This article has not been copyedited and formatted. The final version may differ from this version.

ABCC2 (MRP2), and ABCB5 amongst others (Chen et al., 2009; Frank et al., 2005; Luo et al., 2012; Schadendorf et al., 1995). ABCG2 (BCRP) is also well-characterized and its overexpression causes resistance to a variety of anticancer drugs including paclitaxel and docetaxel(Vlaming et al., 2009; Wu et al., 2011). Additionally, studies have demonstrated that alterations in β-tubulin isotypes can lead to resistance to taxanes in melanoma and other cancers (Hari et al., 2003; Kamath et al., 2005; Mhaidat et al., 2008; Ranganathan et al., 1998). The colchicine binding site is located at the interface between the α- and β-tubulin monomers, and agents that bind to this site may have important advantages over other tubulin inhibitors targeting the taxane or vina alkaloid binding domains. Extensive research efforts have addressed the issue of MDR, and numerous studies have demonstrated that colchicine binding agents can overcome ABCB1(also known as P-glycoprotein) overexpression-, and βIII tubulin-mediated drug resistance (Arnst et al., 2017; Devambatla et al., 2017; Dong et al., 2016; Gangjee et al., 2013; Gangjee et al., 2010; Li et al., 2017b; Stengel et al., 2010; Wang et al., 2012; Wu et al., 2016). While colchicine is not employed as an anticancer agent due to its toxic side effects, other colchicine binding inhibitors have demonstrated promising potential and some are currently being investigated as anticancer candidates (Lu et al., 2012; Stanton et al., 2011).

More recently, there has been increasing interest in the vascular-disrupting capabilities possessed by some microtubule binding agents (Canela et al., 2017; Ji et al., 2015; Schwartz, 2009). It is well-known that tumor progression is dependent on blood vessels to supply oxygen, essential nutrients, and growth factors. Vascular disrupting agents act on the tumor endothelium and induce destructive changes that decrease blood flow, induce vascular collapse, initiate hypoxia within the tumor, and cause necrosis(Canela et al., 2017). There is accumulating evidence that microtubule

Molecular Pharmacology Fast Forward. Published on May 1, 2019 as DOI: 10.1124/mol.118.114801
This article has not been copyedited and formatted. The final version may differ from this version.

binding agents can act selectively on tumor endothelial cells, and this supports the pursuit of targeting tumor vasculature (Schwartz, 2009).

We previously reported a variety of compounds that inhibit tubulin polymerization through interactions with the colchicine binding site. (Ahn et al., 2010; Banerjee et al., 2018; Hwang et al., 2015; Lu et al., 2011; Wang et al., 2012). This led to the development of a novel class of indolyl-imidazopyridines, and several of these compounds demonstrated superior potency *in vitro* and strong tubulin depolymerizing effects (Arnst et al., 2017; Hwang et al., 2015). Herein, we describe one of the most potent of the imidazopyridines, DJ95, and evaluate its potential as a small-molecule chemotherapeutic agent.

DJ95 is highly active against our melanoma panel, as well as many cancer types in the NCI-60 panel. Additionally, it presents a low resistance index against ABC-transporter overexpressing cell lines and outperformed other tubulin targeting agents such as paclitaxel, colchicine, and vincristine. We also evaluated its effect on cancer cell migration, clonogenic potential, and endothelial cell tube formation *in vitro*. Its depolymerization effects were demonstrated through visualization of the microtubule fragmentation as well as the distortion of mitotic spindles. The binding of DJ95 to the colchicine site was confidently confirmed through X-ray crystallographic analyses. Finally, DJ95 inhibited tumor growth *in vivo* in a melanoma xenograft model and did not reveal significant off-target effects in pharmacological screening.

Molecular Pharmacology Fast Forward. Published on May 1, 2019 as DOI: 10.1124/mol.118.114801
This article has not been copyedited and formatted. The final version may differ from this version.

MATERIALS AND METHODS

Cell culture and reagents

Human melanoma cell lines, A375, RPMI-7951, WM-164, WM115 and SK-MEL-1 (American Type Culture Collection or ATCC, Manassas, VA, USA) were cultured in Dulbecco's modified Eagle's medium (DMEM) (Corning, Manassas, VA) supplemented with 10% (v/v) fetal bovine serum (FBS) (Atlanta Biologicals, Lawrenceville, GA) and 1% antibiotic/antimycotic mixture (Sigma-Aldrich, St. Louis MO). HUVEC cells were cultured in Endothelial Cell Growth Medium containing growth supplement (Promocell, Heidelberg, Germany) and 1% antibiotic/antimycotic mixture (Sigma-Aldrich, St. Louis MO). The human epidermoid carcinoma cell line KB-3-1, its drug-selected ABCB1-overexpressing KB-C2 cell line (maintained in medium with 2 μg/mL colchicine) and ABCC1-overexpressing KB-CV60 cell line (maintained in medium with 1 mg/mL of cepharanthine and 60 ng/mL of vincristine) (Wang et al., 2018) were kindly provided by Dr. Shinchi Akiyama at Kagoshima University, Japan. The human non-small cell lung cancer cell line NCI-H460 and its mitoxantrone-selected ABCG2-overexpressing NCI-H460/MX20 cells (maintained in medium with 20 nM of mitoxantrone) (Robey et al., 2001), and the transfected cell lines HEK293/pcDNA 3.1, HEK293/ABCB1, HEK293/ABCC1, and HEK293/ABCG2-R482 were kindly provided by Drs. Susan E. Bates at Columbia University, NY, and Robert W. Robey (NIH, Bethesda, MD). These cell lines were established by transfecting HEK293 cells with either the empty pcDNA3.1 vector or the vector containing full length ABCB1, ABCC1, and wild type ABCG2, respectively(Patel et al., 2017). These cell lines were cultured in DMEM, supplemental with penicillin/streptomycin (Corning, Manassas, VA) and FBS or Hyclone bovine calf serum (GE Healthcare Life Science, Pittsburgh, PA). All cell lines were authenticated by ATCC by short tandem repeat profiling. Cultures were

Molecular Pharmacology Fast Forward. Published on May 1, 2019 as DOI: 10.1124/mol.118.114801
This article has not been copyedited and formatted. The final version may differ from this version.

maintained to 80-90% confluency at 37 °C in a humidified atmosphere containing 5% CO_2. Compounds were dissolved in dimethyl sulfoxide (DMSO) (Sigma-Aldrich, St. Louis, MO) to make a stock solution of 20 mM. Compound solutions were freshly prepared by diluting stocks with cell culture medium before use.

Cytotoxicity assays

The cytotoxic effect against melanoma cell lines was previously described (Arnst et al., 2017). Briefly, A375, RPMI-7951, WM-164, WM115, or SK-MEL-1 cells were seeded in 96-well plates at a density of 1,000–3,500 cells per well, depending on the growth rate of the cell line. After overnight incubation, test compounds were added to the wells at 10 concentrations ranging from 0.03 nM to 1 μM plus a media-only control for 72 h in four replicates. Following treatment, the MTS reagent (Promega, Madison, WI) was added to the cells and incubated in dark at 37 °C for at least 1 hour. Absorbance at 490 nm was measured using a plate reader (BioTek Instruments Inc., Winooski, VT).

The cytotoxic effects of DJ95 to KB-3-1, KB-C2, KB-CV60, NCI-H460 and NCIH460/MX20 cell lines, and the transfected cell lines HEK293/pcDNA3.1, HEK293/ABCB1, HEK293/ABCC1, and HEK293/ABCG2-R482, were determined using the MTT reagent (Thermo Fisher Scientific Inc., Haverhill, MA) as previously described (Fan et al., 2018). Known tubulin inhibitors with different mechanisms of actions, including paclitaxel (microtubule-stabilizing agent, targeting the taxane-binding site in tubulin), colchicine (microtubule-destabilizing agent, targeting the colchicine-binding site in tubulin), and vincristine (microtubule-destabilizing agent, targeting the vinca alkaloid-binding site in tubulin) (Li et al., 2017a; Perez, 2009a), were selected as positive controls for comparison with DJ59. Paclitaxel, colchicine and vincristine, which are existing substrates of ABCB1 and ABCC1(Chen et al.,

Molecular Pharmacology Fast Forward. Published on May 1, 2019 as DOI: 10.1124/mol.118.114801
This article has not been copyedited and formatted. The final version may differ from this version.

2006; Deeley and Cole, 2006; Hodges et al., 2011), also served as positive substrate controls for the experiments involving ABCB1- or ABCC1-overexpressing cell lines in this study. Mitoxantrone, a known substrate of ABCG2 (Homolya et al., 2011), was used as positive substrate control in ABCG2-overexpressing cells. Cisplatin was used as negative control since it is not a substrate of ABCB1, ABCC1 or ABCG2 (Fan et al., 2018).

IC_{50} values were calculated by nonlinear regression analysis using GraphPad Prism (GraphPad Software, San Diego, CA). In addition, DJ95 was evaluated in one dose and five dose assays against the NCI-60 cell line panel by the National Cancer Institute Developmental Therapeutics Program (NCI/DTP).

ATPase assay

The vanadate-sensitive ATPase activity of ABCB1 and ABCG2 using crude membranes of High-five insect cells was determined with the presence of DJ-95 (0 to 10,000 nM) or positive substrate drug by PREDEASY ATPase Kits with modified protocols as previously described (Ambudkar, 1998; Wang et al., 2017b). Paclitaxel and topotecan were selected as positive substrate drugs for ABCB1 and ABCG2, respectively.

Colony forming assay

A375 cells were seeded in 6 well plates (500 cells/well) in replicates of four and incubated at 37 °C overnight. Cells were treated with the compound or media only control and incubated for 10 days. Cells were then fixed with methanol and stained with 0.5% crystal violet. Images were taken, and colony area was quantified with ImageJ software (NIH, Bethesda, MD).

Molecular Pharmacology Fast Forward. Published on May 1, 2019 as DOI: 10.1124/mol.118.114801
This article has not been copyedited and formatted. The final version may differ from this version.

Scratch migration assay

A375 and RPMI7951 cells were seeded in 24 well plates (200,000 cells/well) in replicates of four and incubated overnight. A 200 µL pipette tip was used to scratch a straight line through the cell monolayer to remove an area of cells, then washed several times to remove any debris and uprooted cells. Media was replaced containing equivalent vehicle (DMSO) control or DJ95 at 10 nM or 25 nM concentrations. Images were obtained at the start of the experiment and after 24 hrs with Evos Fl Imaging System (LifeTechnologies, Carlsbad, CA). The analysis was performed with ImageJ software (NIH, Bethesda, MD).

Endothelial cell tube formation assay

Matrigel (Corning, Manassas, VA) was thawed on ice overnight then diluted with serum-free media for a final concentration of 10 mg/mL. Matrigel was plated in 48 well plates and incubated at 37 °C for 1 hour. Low passage number HUVEC cells (<5) in logarithmic growth phase were trypsinized and suspended in endothelial cell growth media. Cells (7 x10^4) were plated on the matrigel plates in quadruplicate containing the desired drug concentrations. Images were captured after 6 hr incubation with Evos Fl Imaging System (LifeTechnologies, Carlsbad, CA). Analysis was performed with angiogenesis tool plug-in with ImageJ software (NIH, Bethesda, MD).

Immunofluorescent staining

WM-164 cells were seeded 2.5×10^5 - 5×10^5 on glass coverslips in 6 well plates and incubated overnight. Media was changed, and cells were treated with DJ95, paclitaxel, or media only control for 18 hrs. Cells were then fixed with 4% paraformaldehyde, permeabilized in 0.1% Triton X (Sigma-Aldrich, St. Louis MO) in Phosphate Buffered Saline (PBS) (Thermo Fisher Scientific Inc., Haverhill, MA) and blocked with 3% Bovine serum albumin (Cell Signaling

Molecular Pharmacology Fast Forward. Published on May 1, 2019 as DOI: 10.1124/mol.118.114801
This article has not been copyedited and formatted. The final version may differ from this version.

Technology, Danvers, MA) prior to staining. Microtubules and mitotic spindles were visualized after incubating with anti-α-tubulin antibody (catalog# 62240) (Thermo Scientific, Rockford, IL) and Alexa Fluor 647 goat anti-mouse IgG (catalog#A21235) (Molecular Probes, Eugene, OR). The coverslips were mounted with Prolong Diamond Antifade mounting media containing DAPI (Invitrogen, Eugene, OR) and images acquired with a Keyence BZ-X700 fluorescence microscope and BZ-X analyzer software (Keyence, Osaka, Japan).

X-ray crystallography

Protein expression and purification

The stathmin-like domain of RB3 (RB3-SLD) from rat was transformed into and over-expressed in *E. coli*. The protein was purified by anion-exchange chromatography (QFF; GE Healthcare, eluted with a 0–200 mM NaCl linear gradient in 20 mM Tris-HCl and 1 mM EGTA (pH 8.0)) and gel filtration chromatography (Superdex 75; GE-Healthcare, 10 mM HEPES(pH 7.2), 150 mM NaCl and 2 mM DTT). The peak fractions from the gel filtration column were concentrated to 10 mg/mL and stored at -80 °C (Charbaut et al., 2001; Dorleans et al., 2009; Wang et al., 2016). The TTL protein from chicken was expressed and purified from an *E. coli* expression system as described previously (Prota et al., 2013). Briefly, the protein was expressed in *E. coli* using Lysogeny broth, purified through Ni- nitrilotriacetic acid affinity chromatography and gel filtration chromatography (buffer: Bis-Tris Propane pH 6.5, 200 mM NaCl, 2.5 mM $MgCl_2$, 5 mM βMe, 1% glycerol). The peak fractions were concentrated to 20 mg/mL and saved at -80 °C. The sodium dodecyl sulfate polyacrylamide gel electrophoresis was performed to check the purity of RB3 and TTL. Porcine brain tubulin (catalog # T-238P) (Cytoskeleton Inc., Denver, CO) was supplied at 10 mg/mL in G-PEM (General tubulin buffer:80 mM PIPES pH 6.9, 2 mM $MgCl_2$, 0.5 mM EGTA and 1 mM GTP) as a frozen liquid and saved at -80 °C until use.

Molecular Pharmacology Fast Forward. Published on May 1, 2019 as DOI: 10.1124/mol.118.114801
This article has not been copyedited and formatted. The final version may differ from this version.

Crystallization and crystal soaking

The previously published process of obtaining crystals of the tubulin-RB3_SLD-TTL (T2R-TTL) complex was applied (Prota et al., 2013; Wang et al., 2017a). In brief, tubulin (10 mg/mL), TTL (20 mg/mL) and RB3 (10 mg/mL) were mixed at the molar ratio of 2:1.3:1.2 (Tubulin: RB3_SLD: TTL) and incubated on ice with 1 mM AMPPCP acid adenylate ester, 5 mM tyrosinol and 10 mM DDT, and the mixture was concentrated to 20 mg/mL at 4 °C. The crystallization of the T2R-TTL complex was carried out at 20 °C using the sitting-drop vapor diffusion method by mixing an equal volume of protein complex and crystallization buffer containing 6% PEG 4000, 5% glycerol, 0.1 M MES, 30 mM $CaCl_2$, 30 mM $MgCl_2$, pH 6.7. Seeding was used to obtain the well diffracting crystals. Initial crystals were observed after two days of incubation and reached a final length of 200-300 μm within 3-5 days. Morphologically superior crystals were selected, cryoprotected with crystallization buffer containing 20% glycerol, and flash frozen in liquid nitrogen.

X-ray data collection and structure determination

Diffraction data were collected at 100K on the beamlines BL19U1 at Shanghai Synchrotron Radiation Facility (SSRF) in Shanghai, China. Data were indexed, integrated and scaled using HKL2000 (Otwinowski and Minor, 1997). The structure of T2R-TTL-DJ95 was determined by molecular replacement using the previously published T2R-TTL structure (PDB ID: 4I55) as a search model. The rotation and translation function searches were performed by the program PHASER (McCoy et al., 2007). The model was further built with Coot (Emsley and Cowtan, 2004) and refined using the phenix.refine module Phenix (Adams et al., 2002). The model quality was checked with PROCHECK and shows a good stereochemistry according to the Ramachandran plot.

Molecular Pharmacology Fast Forward. Published on May 1, 2019 as DOI: 10.1124/mol.118.114801
This article has not been copyedited and formatted. The final version may differ from this version.

Surface plasmon resonance (SPR) for tubulin binding affinity analyses.

To evaluate the binding affinities of DJ95 with tubulin protein, we performed SPR analyses using a Biacore T200 system (GE Healthcare Life Sciences). A Series S Sensor Chip CM5 (GE Healthcare Life Sciences) was pre-conditioned with three consecutive 1-min injections of 70% (w/w) BIA normalizing solution. Then 20 μg/mL tubulin (catalog # T-238P) (Cytoskeleton Inc., Denver, CO) was immobilized to the sensor chip surface to attain 17,000RU (1,000 RU correspond to an angle change of ~0.1°). One of the four flow cells on the chip was left free as a negative control. DJ95, colchicine or CA-4 (positive controls) was injected over the sensor chip surface for association analysis, followed by dissociation analysis. We adjusted the concentration gradients for each of the three compounds based on their different affinities to tubulin and different solubility. The experiment data were obtained at 25°C with running a buffer PBS (10 mM phosphate, 2.7 mM KCl, 137 mM NaCl), and 0.01% (v/v) surfactant P20, pH7.4. The flow rate was 30 μl/min. The analytes bound on the sensor chips were connected for 120 s and dissociated for 120 s. Regeneration of the sensor chips was performed for 30 s by 10 mM glycine-HCl buffer (pH = 1.5). The equilibrium dissociation constant (Kd) was calculated by a steady state fitting mode with Biacore T200 Evaluation Software, version 2.

***In vitro* pharmacological profiling to assess potential off-target effects**

Screening of potentially significant off-target effects to DJ95 binding and enzyme targets was performed via SafetyScreen44 offered by Eurofins Cerep-Panlabs. DJ95 was tested at 100 nM. Compound binding was calculated as a % inhibition of the binding of a radioactively labeled ligand specific for each target. Compound enzyme inhibition effect was calculated as a % inhibition of control enzyme activity. Results showing an inhibition (or stimulation for assays run in basal conditions) higher than 50% are considered to represent significant effects of the test

Molecular Pharmacology Fast Forward. Published on May 1, 2019 as DOI: 10.1124/mol.118.114801
This article has not been copyedited and formatted. The final version may differ from this version.

compounds. Results showing an inhibition (or stimulation) between 25% and 50% are indicative of weak effects. Results showing an inhibition (or stimulation) lower than 25% are not considered significant and mostly attributable to variability of the signal around the control level. In each experiment, the respective reference compound was tested concurrently with DJ95, and the data were compared with historical values determined at Eurofins. The experiment was accepted in accordance with Eurofins validation Standard Operating Procedure.

LC-MS/MS plasma concentration analysis

LC-MS/MS parameters

The LC-MS/MS system comprised a Sciex (Framingham, MA) 5500 triple quadrupole mass spectrometer, equipped with a Turboionspray™ ionization interface and Analyst software version 1.6.3. Chromatographic separation was carried out using a ZORBAX SB-C18 column of 150 x 4.6 mm i.d., and 3.5 µm particle size (Agilent Technologies, Santa Clara, CA) maintained at 35°C using Shimadzu (Columbia, MD) Nexera XR HPLC system and SIL-20ACXR autosampler. The mobile phase (A: Milli-Q water, B: methanol) was eluted at a flow rate of 0.5 mL/min. The gradient started at 50% of mobile phase B and maintained for 0.5 min , then linearly rose to 100 % B over 1 min. Subsequently, the eluent composition was maintained at 100% B from 1.5 to 6 min before it was decreased to initial condition 50 % mobile phase B for re-equilibration in 0.1 min. The total run time was 6.5 min plus a pre-equilibrate of 0.5 min. A switching valve directed the mobile phase to the MS system between 4.5 and 6.1 min. The electrospray ion source was operated in a positive ionization mode for all the experiments. The typical parameters were: capillary 5.5 kV; entrance potential (EP) 10 V; channel electron multiplier (CEM) 1800 V; source temperature 600°C. Other compound specific parameters are listed in Supplement Table 1.

Molecular Pharmacology Fast Forward. Published on May 1, 2019 as DOI: 10.1124/mol.118.114801
This article has not been copyedited and formatted. The final version may differ from this version.

LC-MS/MS sample preparation

Protein precipitation was used to extract DJ95 from plasma. Plasma (50 µL) was added in 150 µL precipitation solution, methanol including 26.5 nM ABI-231 as IS, vortexed for 15 seconds, and then centrifuged for 15 minutes at 4°C (circa 12,000 rpm). Supernatant (120 µL) was then transferred to a 96-well plate and 1 µL sample was injected into the LC-MS/MS system.

Calibration standards were prepared by mixing DJ95 stock solution in pooled human plasma, resulting in matrix concentrations of 1, 10, 100, 200, 1000, 2000, 10,000 nM. Blank samples were prepared using blank plasma. All samples were stored at -20°C prior to use. The lowest standard of 1 nM was not detected. The LLOQ was determined to be 10 nM.

***In vivo* mouse models and treatments**

All protocols and methods, including methods of anesthesia, administration of drugs, blood collection and endpoints requiring euthanasia, were approved by the University of Tennessee Health Science Center (UTHSC) Animal Care and Use Committee (ACUC), consistent with the *Guide for the Care and Use of Laboratory Animals*, 8th edition as published by the National Academy of Sciences. All animals were maintained in a room with a 12 h light/dark cycle and provided food and water ad libitum.

Pharmacokinetic studies

Thirty CD-1 ICR mice from Charles River Laboratories (Wilmington, MA) of approximately 6 weeks of age were used for the study. A mix of males and females were used, and at least one animal of each sex was collected at each time point. For each time point cohort, animals (n=3 per time point) were dosed with 15 mg/kg DJ95 via intraperitoneal injection and the drug vehicle was PEG300 (Sigma-Aldrich, St. Louis MO) and PBS at a 1:1 ratio.

Molecular Pharmacology Fast Forward. Published on May 1, 2019 as DOI: 10.1124/mol.118.114801
This article has not been copyedited and formatted. The final version may differ from this version.

Blood was collected using heparinized syringes from mice deeply anesthetized with isoflurane during the terminal blood collection via cardiac venipuncture into lithium heparinized tubes. At each time point, blood (~0.6 mL) was collected from a separate cohort of three mice at the following time points: 0, 15, 30, 60, 90, 180, 260, 480, 720 and 1440 minutes. Samples were centrifuged at 3,000 rpm for 10 min. Plasma was collected into 1.5mL centrifuge tubes and frozen at -80°C until analysis by LC/MS. Pharmacokinetic parameters were determined by noncompartmental analysis using Phoenix WinNonlin 8.1 (Certara, Princeton, NJ). These parameters included area under the concentration-time profile curve (AUC), half-life ($t_{1/2}$), clearance, volume of distribution and maximum concentration (C_{max}).

MTD and Xenograft study

Nude mice, 50:50 male:female, age 6–8 weeks old, were purchased from Evigo Laboratories (Indianapolis, IN). A maximum tolerable dose (MTD) study was performed by subjecting nude mice up to a dose of 30 mg/kg of DJ95 formulated in the vehicle (equal parts PEG300:PBS) by i.p. injection for 5 consecutive days. Because mice began to show signs of toxicity beyond 30 mg/kg for the 5 day treatment, we scaled the dose back to 15mg/kg for the xenograft study to ensure an adequate safety margin. Logarithmic growth phase A375 cells were prepared in phenyl red-free, FBS-free media and mixed with thawed matrigel prior to injecting into mice. Tumors were established by injecting 100 μL of matrigel/cell suspension containing 2.5×10^6 cells subcutaneously in the hind flank of each mouse. After tumors were established, mice were ranked on tumor size and randomized into control or treatment groups, with each group receiving half males and half females. 100 μL of the drug treatment or vehicle control solution was administered via i.p. injection 5 times a week for the duration of the studies.

Molecular Pharmacology Fast Forward. Published on May 1, 2019 as DOI: 10.1124/mol.118.114801
This article has not been copyedited and formatted. The final version may differ from this version.

Tumor volume was measured three times a week with a caliper and calculated by using the formula a×b2×0.5, where a and b represent the larger and smaller diameters, respectively. Tumor growth inhibition (TGI) at the conclusion of the experiments was calculated as 100 – 100 ×((T − T0)/(C − C0)), where T, T0, C and C0 are the mean tumor volume for the specific group on the last day of treatment, mean tumor volume of the same group on the first day of treatment, mean tumor volume for the vehicle control group on the last day of treatment and mean tumor volume for the vehicle control group on the first day of treatment, respectively (Wang et al., 2014). Animal activity was monitored, and body weights were recorded throughout the study to assess potential acute toxicity. At the end of the experiment, mice were sacrificed, and the tumors were dissected out, weighed, and fixed in in 10% neutral buffered formalin solution prior to pathology staining analysis.

Histology and immunohistochemistry

The fixed tumor xenograft tissues were embedded in paraffin. Serial sections were obtained for immunohistochemistry analysis. Staining was performed with rabbit anti-CD31 (catalog # D8V9E) (Cell Signaling Technology Inc., Danvers, MA) following ABC-DAB methods. Antigen retrieval was performed with H-3300 antigen unmasking solution (Vector Laboratories, Burlingame, CA). Images were captured with a Keyence BZ-X fluorescent microscope (Keyence Corporation, Itasca, IL) at 10x and 20x magnification. Five representative fields of view from three tumors per group at 20x magnification were analyzed in ImageJ to calculate positive stained area.

Statistical analysis

In all studies, it was presumed that the null hypothesis would be that the DJ95 treatment had no effect on the biological phenotype measured compared to the control, therefore, significance was

Molecular Pharmacology Fast Forward. Published on May 1, 2019 as DOI: 10.1124/mol.118.114801
This article has not been copyedited and formatted. The final version may differ from this version.

based on two-tailed statistics tests. The sample sizes for all in vitro and in vivo studies were pre-determined before the studies were initiated. *In vitro* studies included multiple technical replicates per assay and were repeated at least three times (biological replicates). IC_{50} values were calculated by nonlinear regression and SD was determined from at least 3 independent experiments. For in vivo studies, sample sizes were based on our prior experience from studies testing similar drug compounds in xenograft animal models using the subcutaneous injection method. For in vitro experiments comparing multiple doses of DJ95 multiple doses (Figures 2, 8), the statistical significance ($p < 0.05$) was calculated by one-way analysis of variance (ANOVA) followed by Dunnett's multiple comparison test. For the in vivo experiments (Figure 7), two cohorts were compared to each other, the control mice (vehicle, n=7) and the DJ95-treated mice (15 mg/kg, n=6) using the unpaired Student's *t*-test. Data for endpoint tumor volume and tumor wet weight were shown as a scatter plot presenting the mean with one SD. All data were analyzed using Prism Software 5.0 (GraphPad Software, Inc., San Diego, CA).

Molecular Pharmacology Fast Forward. Published on May 1, 2019 as DOI: 10.1124/mol.118.114801
This article has not been copyedited and formatted. The final version may differ from this version.

RESULTS

DJ95 is potent against cancer cell lines and overcomes ABC transporter-mediated resistance.

We previously reported that DJ95 is active against a variety of melanoma and prostate cancer cell lines (Hwang et al., 2015). To further explore these initial findings, we tested DJ95 against a panel of malignant melanoma cell lines representing genomic complexity and heterogeneity, including A375, RPMI-7951, WM-164, WM115, and SK-MEL-1 (Supplement Table 2). We discovered that DJ95 was highly potent in melanoma cell lines and had IC_{50} values of less than 100 nM (Table 1). It was the most potent against A375, with an average IC_{50} of 24.7 ± 4.9 nM and was similar to colchicine (10.6 ± 1.8 nM). Paclitaxel was generally the most potent against the parental melanoma cell lines.

Because we were particularly interested in the ability of DJ95 to overcome transporter-mediated drug resistance, we tested DJ95 against genetically engineered HEK293 cells lines, that stably transfected full length ABCB1, ABCC1, wild type ABCG2, or the pcDNA3.1 blank vector (Supplement Figure 1). Cisplatin, which is not a substrate for any of these ABC transporters, was used as negative control. Greater than 100-fold resistance was observed for the ABCB1 overexpressing HEK293 cells against paclitaxel, and colchicine and vincristine (Table 2). On the other hand, HEK293/ABCB1 resistant cells showed virtually no resistance to DJ95. Slight resistance (RI= 3.7) was revealed for the ABCC1 overexpressing HEK293 transfected cells against DJ95 compared to the vector-only cells, but all other microtubule targeting drugs that were tested (paclitaxel, colchicine, vincristine) demonstrated significantly increased resistance, with IC_{50}s greater than 10,000 nM against HEK293/ABCC1. Similarly, against the HEK293/ABCG2-R482 cells, resistance was evident for all tubulin inhibitors, though less

Molecular Pharmacology Fast Forward. Published on May 1, 2019 as DOI: 10.1124/mol.118.114801
This article has not been copyedited and formatted. The final version may differ from this version.

resistance was developed against the DJ95 compound (about 8.7-fold). This was still lower than mitoxantrone, a known substrate of ABCG2, showing about 11.2-fold decrease in potency in the ABCG2 over-expressing cell line.

We also wanted to assess the effects of DJ95 against drug-selected, resistant cell lines. From the parental epidermoid carcinoma cell line KB-3-1, the colchicine resistant/ABCB1-overexpressing (KB-C2) cell line and vincristine resistant/ABCC1-overexpressing (KB-CV60) cell line were developed. The mitoxantrone-selected ABCG2-overexpressing cell line NCI-H460/MX20 generated from the parental non-small cell lung cancer cell line NCI-H460 was utilized to further evaluate the effects against ABCG2 upregulation. Overexpression of ABCB1, ABCC1, or ABCG2 for each of these cell lines is shown in Supplement Figure 1.

Compared to existing tubulin inhibitors paclitaxel, colchicine and vincristine, DJ95 exhibited higher cytotoxic levels in drug-selected ABCB1-overexpressing KB-C2 cells and ABCC1-overexpressing KB-CV60 cell lines, with IC_{50} values of 719.54 ± 181.48 nM and 35.90 ± 4.50 nM, respectively (Table 3). Although there was still some increase in resistance against the KB-C2 (colchicine selected/ABCB1 over-expressing) cells compared to the parental KB-3-1 cells, both KB-C2 and KB-CV60 were much less resistant to DJ95 than they were against the three other tubulin inhibitors tested. Since no resistance to DJ95 was revealed from ABCB1 transfected cell line, the increase in resistance observed for DJ95 against the colchicine-selected KB-C2 may be related to mechanisms affiliated with the colchicine binding site and not solely ABCB1 overexpression.

In both NCI-H460 and its mitoxantrone-selected ABCG2 overexpressing cell line, DJ95 demonstrated better anti-cancer activities than paclitaxel, colchicine and vincristine, with IC_{50} values of 673.04 ± 111.71 nM and 5361.50 ± 645.45 nM, respectively, whereas IC_{50} values of

Molecular Pharmacology Fast Forward. Published on May 1, 2019 as DOI: 10.1124/mol.118.114801
This article has not been copyedited and formatted. The final version may differ from this version.

the three other tubulin inhibitors were higher than 10,000 nM in both cell lines. However, low resistance against DJ95 was observed in NCI-H460/MX20 cell line compared to its parental cell line (about 8-fold resistance), though the resistance index was not as high as that of the substrate control mitoxantrone (about 20-fold resistance). The resistance index is the ratio of IC_{50} value of the drug resistant cell (or transfected cell overexpressing ABC transporter) over IC_{50} value of the parental cell (or vector control for the transfected cell). The results from the drug-selected resistant cells are consistent with those obtained from transfected ABCG2-overexpressing cell line HEK293/ABCG2-R482 and its vector control, which indicated that DJ95 might be a weak substrate of ABCG2.

To follow up on these results, the ABCB1 or ABCG2 ATPase activity with the presence of DJ95 were investigated to assess the interaction between DJ95 and these ABC transporters. DJ95 inhibited ABCB1-mediated ATP hydrolysis, while paclitaxel, which is a substrate of ABCB1, stimulated the vanadate-sensitive ATPase activity of ABCB1 (Supplement Figure 2A). This suggests that DJ95 may not be a substrate of ABCB1 and may be able to circumvent ABCB1-medited MDR, which is consistent with the cytotoxicity results from HEK293/ABCB1 and HEK293/pcDNA3.1 cells. On the contrary, DJ95 showed stimulating effects on ABCG2 ATPase activity, similarly to the positive substrate drug, topotecan (Supplement Figure 2B). This is in accordance with the resistance to DJ95 shown by ABCG2-overexpressing cells, which further supports the hypothesis that DJ95 may be a substrate of ABCG2.

Finally, DJ95 was tested in the NCI-60 screening, assaying a diverse selection of cancer types. DJ95 was evaluated in a single-dose assay (Supplement Figure 3A and S3B) as well as a 5-concentration assay to see if it was sensitive in other kinds of cancer (Figure 1). DJ95 was highly active and demonstrated a low GI_{50} for the majority of melanoma cell lines, and was especially

Molecular Pharmacology Fast Forward. Published on May 1, 2019 as DOI: 10.1124/mol.118.114801
This article has not been copyedited and formatted. The final version may differ from this version.

effective against leukemia, colon, CNS, and prostate cancers. The average total growth inhibition (TGI) and LC_{50} was greatest for colon cancer and melanoma. Additionally, we assessed the dose-response curves of each individual melanoma cell line tested and determined that the cell lines most sensitive to DJ95 treatment were LOX IMVI and SK-MEL-5 (Supplement Figure 3C, Supplement Table 3). Together, these results indicate that DJ95 is effective against a multitude of cancer cell lines representing genomic heterogeneity, drug resistant profiles, and cancer types.

DJ95 impedes cancer cell colony formation and migration.

After verifying the potency of DJ95, it was further evaluated for functional inhibition of cell proliferation and migration *in vitro*. We first determined its ability to inhibit colony formation in a concentration-dependent manner compared to untreated A375 control cells (Figure 2A). A significant decrease was observed for all treated cells, and concentrations as low as 10 nM caused a 26.78 ± 1.9% inhibition of colony area compared to control ($P < 0.001$) and higher concentrations of 25 nM and 50 nM inhibited colony formation by 44.73 ± 1.9% and 65.01 ± 3.08%, respectively ($P <0.0001$) (Figure 2B). At 100 nM, DJ95 almost completely eliminated colony formation and only 1.25 ± 0.07% of the area compared to the control remained. DJ95 was then tested in both A375 and RPMI-7951 melanoma cell lines to determine its effect on migration ability of the cells in a scratch assay (Figure 2C). After 24 hrs, the untreated cells migrated into 80.73 ± 4.48% of the wound channel, nearly closing the gap. Treatment to the A375 cells with 10 nM and 25 nM of DJ95 decreased the cell migration and led to cells only occupying 58.23± 2.15% ($P < 0.01$) and 35.60 ± 1.35% ($P < 0.0001$) of the scratch area, which was significantly less than the control (Figure 2D). A similar phenomenon was also observed in the RPMI-7951 cell line, where the control cells reclaimed 77.43 ± 3.91% of the scratch area

Molecular Pharmacology Fast Forward. Published on May 1, 2019 as DOI: 10.1124/mol.118.114801
This article has not been copyedited and formatted. The final version may differ from this version.

(Figure 2E). Treatments of 10 nM and 25 nM of DJ95 caused the cells to only migrate into 34.37 ± 6.09% ($P < 0.001$) and 23.10 ± 2.92% ($P < 0.0001$) of the scratch area, respectively. There was no significant difference in the scratch channel area for each group at the beginning of the experiment (time 0) as determined by two-way ANOVA analysis factoring in both time and treatment group (Supplement Figure 4). To this end, it can be interpreted that DJ95 inhibits cell proliferation and migration at low concentrations for these melanoma cell lines.

DJ95 disrupts microtubule networks and mitotic spindle formation.

Previously, we demonstrated that DJ95 is able to potently inhibit polymerization of purified tubulin protein in a cell-free assay (Hwang et al., 2015). Here, we visually present the effect DJ95 has on the microtubule networks of WM-164 melanoma cells (Figure 3A). The stabilizing agent paclitaxel, a potent enhancer of polymerization, was also used for comparison. After 18 hrs of treatment at a 50 nM concentration with DJ95, cells showed dramatically disrupted microtubule networks and an increase in soluble, cytoplasmic tubulin. Furthermore, at 200 nM, there appears to be very little polymeric tubulin framework left intact. In contrast, paclitaxel treated cells demonstrated highly condensed, polymeric tubulin. For cells treated at the higher concentration of 200 nM paclitaxel, the fluorescent signal was amplified and the aggregation of the filaments was more pronounced, consistent with increased stabilization of microtubules.

Microtubules also make up the mitotic spindle and utilize the dynamic properties for chromosome segregation during mitosis (Kline-Smith and Walczak, 2004). Therefore, tubulin targeting agents also interfere with the formation and organization of mitotic spindles (Rai et al., 2012; Rohena et al., 2016; Sakchaisri et al., 2017; Weiderhold et al., 2006). We investigated the effects of DJ95 in a concentration-dependent manner compared to untreated control cells (Figure

Molecular Pharmacology Fast Forward. Published on May 1, 2019 as DOI: 10.1124/mol.118.114801
This article has not been copyedited and formatted. The final version may differ from this version.

3B). While control cells exhibited normal, bilateral spindle formation extruding from centrosomes, DJ95 treatment led to aberrant spindle development as evidenced by multi-polar and disorganized spindle morphology. These abnormalities were exacerbated with increasing drug concentrations. This is further proof that DJ95 inhibits the progression of mitosis by interfering with microtubule dynamics.

X-ray crystallography confirms that DJ95 occupies the colchicine binding site.

We determined the crystal structure of the T2R-TTL complex bound with compound DJ95 at 2.4 Å resolution (Figure 4A), and the coordinates and structure factors have been deposited in the Protein Data Bank with the PDB ID: 6NNG. The refinement statistics and overall geometric parameters confirm that the structure quality is excellent; this information together with the data collection parameters are presented in Table 4. DJ95 binds at the interface of the α/β-tubulin heterodimer and occupies the same locale as colchicine in the β-tubulin protomer (PDB ID: 4O2B) directly opposite the GTP that binds within the α-tubulin. Unlike colchicine that binds both available α/β interfaces in the T2R-TTL complex, DJ95 only binds to the interface proximal to the TTL subunit. DJ95 is slightly more extended than colchicine and it appears that the single occupancy is not biologically relevant but rather the result of small conformational changes in the assembly that cannot easily be accommodated by the packing within the crystal lattice. The 3-methoxyphenyl group of DJ95 occupies a deep pocket that is lined with residues Tyr200, Val236, Cys239, Leu240, Leu250, Leu253, Ala314, Ile316, Ala352 and Ile368 (Figure 4B). The central imidazopyridine ring and the distal indole ring are linearly connected and flanked on one side by residues from the short α-helix β-H8, specifically Lys252, Leu253, Asn256 and Met257, and residues Lys350 and Leu246 on the other side. The DJ95 binding

Molecular Pharmacology Fast Forward. Published on May 1, 2019 as DOI: 10.1124/mol.118.114801
This article has not been copyedited and formatted. The final version may differ from this version.

interactions are almost exclusively van der Waals in nature but there are several specific interactions (Figure 4B). The central imidazopyridine ring forms two hydrogen bonds; a nitrogen atom with the main chain amide of Asp249, and an NH group with the main chain carbonyl oxygen of Thr179 of α-tubulin across the interface. The 3-methoxyphenyl moiety has three interactions; the central methoxy group interacts via a water molecule with the main chain NH of Cys239, and the side chains of Leu253 and Cys239 make flanking pi-H interactions with the phenyl ring.

Comparison with the colchicine complex reveals that the binding interactions are very similar, with most of the residues described above in equivalent conformations (Figure 4C). There are two noticeable differences. First, the equivalent 3-methoxyphenyl moiety of colchicine does not penetrate the pocket as deeply (by some 2.5 Å) which precludes the water mediated hydrogen bond to the central methoxy group. Second, in the unliganded (PDB ID: 4I55) and colchicine liganded T2R-TTL complexes, the side chain of Lys350 is extended and interacts across the α/β interface with Ser178 and Thr179, respectively, in the flexible α-T5 loop of α-tubulin. In the DJ95 complex, however, steric interference with the distal indole ring and favorable van der Waals interactions with the molecule cause Lys350 to swing around, which in turn allows Thr179 to form the main chain hydrogen bond described above. Finally, in a similar fashion to colchicine, the binding of DJ95 elicits substantial conformational changes at the α/β interface, including within loops β-T7 of β-tubulin and α-T5 of α-tubulin (Figure 4D). These are incompatible with the 'straight' structure of the tubulin filament (PDB ID: 1JFF) and therefore consistent with the DJ95 acting as a destabilizer of filament formation. The electron density map is demonstrated in Supplement Figure 5.

Molecular Pharmacology Fast Forward. Published on May 1, 2019 as DOI: 10.1124/mol.118.114801
This article has not been copyedited and formatted. The final version may differ from this version.

DJ95 shows a lower binding affinity to tubulin than that of colchicine and CA-4.

To quantitatively determine the binding affinity of DJ95 with tubulin protein, we performed surface plasmon resonance experiments using Biacore T200 system (GE Healthcare Life Sciences). A CM5 sensor chip with glucan on the surface was used to immobilize tubulin. DJ95, colchicine or CA-4 was injected over the sensor chip surface for binding detection. As determined by a 1:1 kinetics fitting model, the equilibrium dissociation constant Kd of DJ95, colchicine, and CA-4 was 59.4 μM, 5.7 μM and 7.7 μM, respectively (Figure 5). These data reveal that DJ95 has approximately 10-fold lower binding affinity than colchicine and CA-4, and further modifications will be required to increase the affinity to tubulin and avoid potential binding to additional molecular targets.

DJ95 has negligible interactions with 44 physiologically important targets.

Prior to *in vivo* studies, we wanted to determine if DJ95 would exhibit a relatively safe profile based on interactions with off-targets and predict if there would be any potentially detrimental clinical effects. *In vitro* pharmacological profiling involves screening the compound of interest against a wide range of targets such as receptors, ion channels, transporters and enzymes other than the intended therapeutic target in order to identify specific interactions that may elicit adverse drug-related side effects (Bowes et al., 2012). Here, DJ95 was evaluated in binding and enzyme uptake assays performed by Eurofins Cerep Panlabs. DJ95 demonstrated minimal specific binding inhibition or stimulation against 37 radioactive labeled ligand targets (Figure 6A). Additionally, DJ95 did not induce significant alterations in enzyme function for COX1, COX2, PDE3A, PDE4D2, Lck kinase or ACHE (Figure 6B). Results showing an inhibition or stimulation higher than 50% are considered significant for test compound, none of which were observed at any of the targets studied in this screening. Specific binding assay targets and

Molecular Pharmacology Fast Forward. Published on May 1, 2019 as DOI: 10.1124/mol.118.114801
This article has not been copyedited and formatted. The final version may differ from this version.

enzyme-based assays, along with the corresponding reference compound, are summarized in Supplement Table 4.

DJ95 pharmacokinetics and antitumor activity *in vivo*.

Based on the preliminary *in vitro* data suggesting that DJ95 is potently active against melanoma cell lines and minimally interferes with off-targets, we sought to test the activity of DJ95 *in vivo*. We determined that concentrations up to 30 mg/kg administered by i.p. injection daily was well-tolerated for at least 5 days in nude mice, but additional treatments caused a decrease in mouse weight and decline in behavioral activity. Therefore, we scaled back the dose to half of that (15 mg/kg) for the pharmacokinetic and xenograft study. To determine if DJ95 could reach therapeutically relevant biological concentrations at doses of 15 mg/kg, we collected blood samples from 15 minutes to 24 hrs following i.p. injection of the drug and analyzed the plasma concentrations by LC-MS methods. The C_{max} for DJ95 was 13.65 μM and the detected concentrations stayed above 13 μM for at least 1.5 hrs in mouse plasma (Figure 7A). While the concentration of DJ95 gradually decline over the course of the 24 hrs when samples were collected, there was still an average of 126.5 nM at 12 hrs and 8.1 nM at 24 hrs. This data, along with the AUC (50,500 hr*nM) suggests acceptable exposure for DJ95 over the course of a day. We also determined additional pharmacokinetic parameters including half -life (3.28 hrs), volume of distribution to (3.51 L/kg), and clearance (0.744 L/hr/kg). We reasoned that these results supported a dosing regimen of 5 treatments/week, allowing for 2 recovery days to avoid accumulating toxicities. To test the anticancer efficacy of DJ95 *in vivo*, xenografts were established by subcutaneous inoculation of A375 cells, and treatment began after viable tumors developed. Groups were dosed by i.p. injection with either 15 mg/kg treatments of DJ95 or

Molecular Pharmacology Fast Forward. Published on May 1, 2019 as DOI: 10.1124/mol.118.114801
This article has not been copyedited and formatted. The final version may differ from this version.

vehicle solution only. After two weeks and a total of 10 treatments, tumor growth for the DJ95 treated group was significantly inhibited compared to the control group, with a tumor growth inhibition (TGI) of 61.4% (Figure 7B). A student's T test gave an overall *P* value of 0.0081 based on final percent change and 0.0382 based on final tumor volume volumes (Figure 7C), compared to the control group. Animal behavior and mouse body weights were measured and recorded throughout the course of the experiment to assess for acute toxicities, and major deviations were not observed (Figure 7D). At the end of the study, tumors were resected and weighed, and there was a significant decrease in tumor weight for the DJ95 group ($P = 0.0406$) (Figure 7E). This *in vivo* study demonstrates the antitumor efficacy of DJ95 in a melanoma xenograft model and supports its continued investigation as an anticancer agent.

DJ95 shows vascular disrupting capabilities.

In recent years, there has been extensive research on the vascular disrupting properties of tubulin targeting agents and their ability to selectively target tumor vasculature (Banerjee et al., 2016; Ji et al., 2015; Martel-Frachet et al., 2015; Su et al., 2016; Wang et al., 2012). To see whether DJ95 would exhibit these characteristics, we tested the *in vitro* effect on the formation of capillary-like networks of HUVEC cells plated on matrigel. The matrigel basement membrane allows endothelial cells to form tubules with tight cell-to-cell and cell-to-membrane contacts (Benton et al., 2014). After 6 hrs of incubation, it was clearly observed that both DJ95 and colchicine disrupted the tube cell formation in a concentration-dependent manner (Figure 8A). At concentrations of 100 nM and 200 nM, DJ95 disrupted networks by 35.71 ± 5.62% and 51.81 ± 3.25% ($P < 0.0001$) (Figure 8B). This was similar to the effect observed upon colchicine treatment at the same concentrations, inhibiting HUVEC tube cell formation by 60.43 ± 9.04 %

Molecular Pharmacology Fast Forward. Published on May 1, 2019 as DOI: 10.1124/mol.118.114801
This article has not been copyedited and formatted. The final version may differ from this version.

and 81.59% ± 8.01, respectively ($P < 0.0001$). Since this result was observed in a short timeframe, we expect that the drug action on tube cell formation was not a result of antiproliferative activity.

We also wanted to assess the effect on tumor vasculature from the DJ95 treated xenografts. CD31 staining of tumor sections revealed the change in microvessels of the DJ95 treated group compared to the control group (Figure 8C.) It is apparent that the control group has more abundant and in-tact microvessels throughout the tumors, whereas DJ95 treatment induced vessel fragmentation and decreased overall density and occupied area. Quantification of the positive CD31-stained area revealed that there was a 50.47% decrease in total microvessel area, representing a significant difference ($P= 0.0038$) (Figure 8D). Detailed images used for quantification can be found in Supplement Figure 6. This finding corroborates the *in vitro* results and suggests that the anti-vascular capacities portrayed by DJ95 may contribute to its anticancer efficacy.

Molecular Pharmacology Fast Forward. Published on May 1, 2019 as DOI: 10.1124/mol.118.114801
This article has not been copyedited and formatted. The final version may differ from this version.

DISCUSSION

Importance of overcoming drug resistance.

Melanoma is the most aggressive form of skin cancer and is one of the most rapidly increasing cancers worldwide (Linos et al., 2009). Malignant melanoma is characterized by resistance to chemotherapy and is incurable in most affected patients (Kalal et al., 2017; Wu and Singh, 2011). Despite recent advances in treating melanoma with targeted therapies and immunotherapies, significant obstacles still exist for finding satisfactory treatments. Intrinsic and acquired resistance are the major causes of treatment failure, and it is of utmost importance to discover and develop agents that can overcome drug resistance, improve response rates, and extend survival for melanoma patients.

We previously identified DJ95, a small-molecule synthesized from a series of indolyl-imidazopyridines, that targets the colchicine binding site and showed promising activity *in vitro* (Hwang et al., 2015). Genetic heterogeneity among cancer cell lines of the same cancer type has emphasized the necessity to study multiple cell lines in a panel (Gillet et al., 2011). To expand on its cytotoxic potential, DJ95 was tested against our malignant melanoma cell line panel and demonstrated IC_{50} values ranging from 25-100 nM, confirming its strong activity against a variety melanoma cell lines. We also tested DJ95 against the NCI-60 cell panel, to assess its efficacy against other cancers. The NCI-60 cell panel includes numerous cell lines from nine different tumor types which are extensively characterized. DJ95 had an exceptionally low GI_{50} in the majority of cell lines for all cancer types. In addition to melanoma, DJ95 was particularly active against colon cancers based on the TGI and LC_{50}.

One of the most significant factors that limit the efficacy of chemotherapeutics is the development of MDR. One of the major culprits responsible for contributing to MDR is the

Molecular Pharmacology Fast Forward. Published on May 1, 2019 as DOI: 10.1124/mol.118.114801
This article has not been copyedited and formatted. The final version may differ from this version.

overexpression of ABC transporters such as ABCB1 (P-gp/MDR1), ABCC1 (MRP1), and ABCG2 (BCRP) (Gottesman et al., 2002). Agents that target the taxane and vinca binding sites of tubulin are particularly susceptible to resistance from the overexpression ABCB1 and are effectively effluxed from the cell (Callaghan et al., 2014; Fojo and Menefee, 2007; Xia and Smith, 2012; Yusuf et al., 2003). These agents are also substrates to several ABCC/MRP members that decrease their intracellular concentrations (Dumontet and Jordan, 2010). We discovered that DJ95 had a lower resistance index than the other tested tubulin inhibitors in both the drug-selected and gene-transfected cell lines overexpressing ABCC1. While it did not show resistance to the transfected ABCB1 overexpressing cells, it did show some resistance to KB-C2 drug-selected cell line overexpressing ABCB1. Since DJ95 was considered not as a substrate of ABCB1 based on the data that it did not stimulate ABCB1 ATPase activity, the resistance showed from KB-C2 might be contributed by the more complex MDR mechanisms in drug-selected MDR cells in comparison with gene-transfected cells. As KB-C2 cells were established by continuous selection with colchicine (2 μg/mL), they may have incurred additional drug-resistance mechanisms besides solely ABCB1 upregulation. For example, mutations to the colchicine binding domain on tubulin could account for the cross-resistance to DJ95 or other agents targeting this site. Taken together, we infer that DJ95 may be able to circumvent ABCB1- or ABCC1-mediated MDR but may have reduced efficacy in colchicine-selected drug resistant cases.

Targeting mitotic machinery.

The main function of microtubule targeting agents is to inhibit mitosis through disruption of microtubule dynamics (Mukhtar et al., 2014). While stabilizing agents such as paclitaxel

Molecular Pharmacology Fast Forward. Published on May 1, 2019 as DOI: 10.1124/mol.118.114801
This article has not been copyedited and formatted. The final version may differ from this version.

promote polymerization by blocking the disassembly of GDP-bound tubulin and form stable tubulin polymers, destabilizing agents inhibit this assembly of tubulin into microtubules and promote depolymerization (Field et al., 2014). This phenomenon was observed in DJ95 treated cells, which displayed fragmented microtubules and a dramatic decrease of visible tubulin filaments. On the contrary, paclitaxel treated cells demonstrated rigid and condensed polymeric microtubules. Furthermore, microtubules constitute the mitotic spindle in cells undergoing mitosis. Disruption of the mitotic spindle through suppression of treadmilling and dynamic instability are the primary means by which microtubule inhibitors thwart cellular functions and induce apoptosis (Loong and Yeo, 2014). Typical features of mitotic spindle suppression and aberrant formation such as multiple asters in mitotic cells were evident in the DJ95 treated cells, whereas the control cells demonstrated polar spindle formation and centrally aligned chromosomes.

Optimizing scaffolds through x-ray crystallography.

The crystal structure of the T2R-TTL complex bound with DJ95 provides further evidence to the mechanism of action for the anti-cancer activity of this compound. It binds at the colchicine binding pocket at the interface of α- and β-tubulin heterodimer. Colchicine targets the β subunit of tubulin and keeps it from adopting a straight conformation, thus inhibiting microtubule assembly. The binding of DJ95 also blocked the curve-to-straight conformational change of tubulin by the steric clashes between DJ95 and surrounding secondary structure elements (Figure 4C). Therefore, DJ95 likely shares the same inhibition mechanism as that of colchicine. The crystal structure not only provides the structural basis for the anti-cancer activity of DJ95, it also presents opportunities for designing better analogues of this compound that may show improved

Molecular Pharmacology Fast Forward. Published on May 1, 2019 as DOI: 10.1124/mol.118.114801
This article has not been copyedited and formatted. The final version may differ from this version.

potency. For example, replacing a carbon atom that faces residue Asn347 by a hydrogen bond donor (NH) could pick up an additional hydrogen bond with the main chain C=O of Asn347.

Minimizing failure in drug development.

Reducing the attrition rate of potential pharmaceutical drug candidates is an important step in drug discovery and development. Identification of off-target, adverse drug reactions to important pharmacological targets such as GPCRs, drug transporters, ion channels, nuclear receptors, kinases and non-kinase enzymes can aid in determining if a drug may elicit side effects that would prevent its further advancement. Use of predictive safety panels that implement assays to identify significant off-target interactions of drug candidates is supported by major pharmaceutical companies such as AstraZeneca, GlaxoSmithKline, Novartis and Pfizer (Bowes et al., 2012). DJ95 underwent this pharmacological profiling in Eurofins SafetyScreen44™ Panel. DJ95 did not show significant inhibition or activation to any of the 44 physiologically important targets tested in the screening. This suggests that DJ95 minimally interacts with or activates some of the key targets that potentially cause adverse drug reactions. We therefore proceeded with *in vivo* studies and found that DJ95 effectively inhibited melanoma tumor growth at a 15 mg/kg dose. While colchicine is known to cause significant toxicity, no toxic side effects based on animal body weight and behavior were observed in the DJ95 treated groups.

DJ95 disrupts tumor vasculature

It is well-known that tumor growth and metastasis require a reliable system of blood vessels to support the tumor microenvironment, and interfering with this process is an attractive strategy for inhibiting tumor growth (Banerjee et al., 2016; Matter, 2001). This has prompted research in

Molecular Pharmacology Fast Forward. Published on May 1, 2019 as DOI: 10.1124/mol.118.114801
This article has not been copyedited and formatted. The final version may differ from this version.

the development of anti-angiogenic and vascular disrupting agents, and many tubulin inhibitors that target the colchicine binding site demonstrate this capability (Arnst et al., 2017; Banerjee et al., 2016; Galmarini et al., 2018; Ji et al., 2015; Wang et al., 2012). Microtubule stabilizing agents such as paclitaxel, peloruside A, and laulimalide also have reported vascular disrupting properties, but they have other shortcomings, such development of resistance and dose-limiting toxicities (Akiyama et al., 2012; Bocci et al., 2013; Chan et al., 2015; Kanakkanthara et al., 2014). Here, we demonstrate the ability of DJ95 in suppressing capillary-like networks *in vitro* in HUVEC cells in a concentration-dependent manner. We also discovered vascular disrupting action evident in mouse xenografts after DJ95 treatment, where there was significant disturbance of endothelial vasculature and an overall decrease in microvessel area. These *in vitro* and *in vivo* data also support the notion of DJ95 as potential dual inhibitor that may exert its anticancer effects through multiple mechanisms.

Conclusions

In summary, we report the preclinical evaluation of DJ95. DJ95 is effective against a variety of melanoma cell lines and other cancer types, significantly reduces tubulin polymerization, binds to the colchicine binding site on tubulin, and reduces melanoma tumor growth *in vivo* without causing toxicity, and has vascular disrupting properties. DJ95 incurred less resistance in ABC-transporter overexpressing cell lines and could prove to be an effective alternative treatment when other tubulin targeting agents fail to show efficacy due to MDR. There are currently no colchicine binding site agents approved for chemotherapy, and DJ95 shows great potential for the further development as an anticancer agent.

Molecular Pharmacology Fast Forward. Published on May 1, 2019 as DOI: 10.1124/mol.118.114801
This article has not been copyedited and formatted. The final version may differ from this version.

ACKNOWLEDGMENTS

The authors thank Dr. Benoît Gigant (Institute for Integrative Biology of the Cell (I2BC), CEA, CNRS, Univ. Paris-Sud, Universite´ Paris-Saclay, France) and Dr. Michel O. Steinmetz (Paul Scherrer Institute, Switzerland) for kindly providing the plasmids of RB3-SLD and TTL. We thank Dr. Shinichi Akiyama (Kagoshima University, Japan) for kindly provided the KB-3-1, KB-C2 and KB-CV60 cell lines. We are thankful to Drs. Susan E. Bates (Columbia University, NY, USA) and Robert W. Robey (NIH, Bethesda, MD, USA) for generously providing the NCI-H460, NCI-H460/MX20, HEK293/pcDNA 3.1 and the transfected cell lines HEK293/ABCB1, HEK293/ABCC1 and HEK293/ABCG2-482R. We also thank Dr. Yi Xue at UTHSC for helping with the IHC analyses and Dr. Pradeep Lukka for his help with the LCMS analysis of the plasma samples.

Funding.

This work is supported by NIH/NCI grant [R01CA148706] to WL and DDM; NIH grants [1S10OD010678-01] and [1S10RR026377-01] to WL. Other support from grants includes [1S10OD016226-01A1]. Its contents are solely the responsibility of the authors and do not necessarily represent the official views of the NIH. Additional support from the University of Tennessee College of Pharmacy Drug Discovery Center. The X-ray work was partially supported by National Natural Science Foundation of China (Grant No. [81703553]) to YW, QC, and JY. No NIH funds were used for any experiments contributed by YW, QC and JY to this work. All intellectual properties are owned by the University of Tennessee Health Science Center. GK and SWW acknowledge the support of American Lebanese Syrian Associated Charities (ALSAC).

Molecular Pharmacology Fast Forward. Published on May 1, 2019 as DOI: 10.1124/mol.118.114801
This article has not been copyedited and formatted. The final version may differ from this version.

AUTHORSHIP CONTRIBUTIONS

Participated in research design: Arnst, Wang, Miller, Li

Conducted experiments: Arnst, Wang, Lei, Ma, Parke

Contributed to reagents or analytical tools: Arnst, Wang, Lei, Hwang, Seagroves, Q. Chen, Yang, ZS Chen, Li

Wrote or contributed to writing of manuscript: Arnst, Lei, Kumar, White, Li

Conflict of Interest Disclosure: Dr. Wei Li started in January 2019 to serve as a consultant to Veru Inc., who licensed the patent portfolios covering DJ95 and its related analogs for commercial development. Veru Inc. did not provide any financial support or have any influence on research design, experiments, data collection, data analyses, or the writing of this manuscript.

REFERENCES

Adams PD, Grosse-Kunstleve RW, Hung LW, Ioerger TR, McCoy AJ, Moriarty NW, Read RJ, Sacchettini JC, Sauter NK and Terwilliger TC (2002) PHENIX: building new software for automated crystallographic structure determination. *Acta crystallographica Section D, Biological crystallography* **58**(Pt 11): 1948-1954.

Ahn S, Duke CB, 3rd, Barrett CM, Hwang DJ, Li CM, Miller DD and Dalton JT (2010) I-387, a novel antimitotic indole, displays a potent in vitro and in vivo antitumor activity with less neurotoxicity. *Mol Cancer Ther* **9**(11): 2859-2868.

Akiyama K, Ohga N, Hida Y, Kawamoto T, Sadamoto Y, Ishikawa S, Maishi N, Akino T, Kondoh M, Matsuda A, Inoue N, Shindoh M and Hida K (2012) Tumor endothelial cells acquire drug resistance by MDR1 up-regulation via VEGF signaling in tumor microenvironment. *The American journal of pathology* **180**(3): 1283-1293.

Ambudkar SV (1998) Drug-stimulatable ATPase activity in crude membranes of human MDR1-transfected mammalian cells. *Methods in enzymology* **292**: 504-514.

Arnst KE, Wang Y, Hwang D-J, Xue Y, Costello T, Hamilton D, Chen Q, Yang J, Park F, Dalton JT, Miller DD and Li W (2017) A potent, metabolically stable tubulin inhibitor targets the colchicine binding site and overcomes taxane resistance. *Cancer research*.

Banerjee S, Arnst KE, Wang Y, Kumar G, Deng S, Yang L, Li G-b, Yang J, White SW, Li W and Miller DD (2018) Heterocyclic-Fused Pyrimidines as Novel Tubulin Polymerization Inhibitors Targeting the Colchicine Binding Site: Structural Basis and Antitumor Efficacy. *Journal of medicinal chemistry* **61**(4): 1704-1718.

Banerjee S, Hwang DJ, Li W and Miller DD (2016) Current Advances of Tubulin Inhibitors in Nanoparticle Drug Delivery and Vascular Disruption/Angiogenesis. *Molecules (Basel, Switzerland)* **21**(11).

Benton G, Arnaoutova I, George J, Kleinman HK and Koblinski J (2014) Matrigel: from discovery and ECM mimicry to assays and models for cancer research. *Advanced drug delivery reviews* **79-80**: 3-18.

Bocci G, Di Paolo A and Danesi R (2013) The pharmacological bases of the antiangiogenic activity of paclitaxel. *Angiogenesis* **16**(3): 481-492.

Bowes J, Brown AJ, Hamon J, Jarolimek W, Sridhar A, Waldron G and Whitebread S (2012) Reducing safety-related drug attrition: the use of in vitro pharmacological profiling. *Nature reviews Drug discovery* **11**(12): 909-922.

Callaghan R, Luk F and Bebawy M (2014) Inhibition of the multidrug resistance P-glycoprotein: time for a change of strategy? *Drug metabolism and disposition: the biological fate of chemicals* **42**(4): 623-631.

Canela MD, Noppen S, Bueno O, Prota AE, Bargsten K, Saez-Calvo G, Jimeno ML, Benkheil M, Ribatti D, Velazquez S, Camarasa MJ, Diaz JF, Steinmetz MO, Priego EM, Perez-Perez MJ and Liekens S (2017) Antivascular and antitumor properties of the tubulin-binding chalcone TUB091. *Oncotarget* **8**(9): 14325-14342.

Chan A, Singh AJ, Northcote PT and Miller JH (2015) Inhibition of human vascular endothelial cell migration and capillary-like tube formation by the microtubule-stabilizing agent peloruside A. *Investigational new drugs* **33**(3): 564-574.

Charbaut E, Curmi PA, Ozon S, Lachkar S, Redeker V and Sobel A (2001) Stathmin family proteins display specific molecular and tubulin binding properties. *The Journal of biological chemistry* **276**(19): 16146-16154.

Chen KG, Valencia JC, Gillet JP, Hearing VJ and Gottesman MM (2009) Involvement of ABC transporters in melanogenesis and the development of multidrug resistance of melanoma. *Pigment cell & melanoma research* **22**(6): 740-749.

Chen Q, Yang Y, Li L and Zhang J-T (2006) The amino terminus of the human multidrug resistance transporter ABCC1 has a U-shaped folding with a gating function. *Journal of Biological Chemistry* **281**(41): 31152-31163.

Deeley RG and Cole SPC (2006) Substrate recognition and transport by multidrug resistance protein 1 (ABCC1). *FEBS Letters* **580**(4): 1103-1111.

Devambatla RKV, Li W, Zaware N, Choudhary S, Hamel E, Mooberry SL and Gangjee A (2017) Design, synthesis, and structure-activity relationships of pyrimido[4,5-b]indole-4-amines as microtubule depolymerizing agents that are effective against multidrug resistant cells. *Bioorganic & medicinal chemistry letters* **27**(15): 3423-3430.

Dong M, Liu F, Zhou H, Zhai S and Yan B (2016) Novel Natural Product- and Privileged Scaffold-Based Tubulin Inhibitors Targeting the Colchicine Binding Site. *Molecules (Basel, Switzerland)* **21**(10).

Dorleans A, Gigant B, Ravelli RB, Mailliet P, Mikol V and Knossow M (2009) Variations in the colchicine-binding domain provide insight into the structural switch of tubulin. *Proceedings of the National Academy of Sciences of the United States of America* **106**(33): 13775-13779.

Dumontet C and Jordan MA (2010) Microtubule-binding agents: a dynamic field of cancer therapeutics. *Nature reviews Drug discovery* **9**(10): 790-803.

Emsley P and Cowtan K (2004) Coot: model-building tools for molecular graphics. *Acta crystallographica Section D, Biological crystallography* **60**(Pt 12 Pt 1): 2126-2132.

Fan Y-F, Zhang W, Zeng L, Lei Z-N, Cai C-Y, Gupta P, Yang D-H, Cui Q, Qin Z-D and Chen Z-S (2018) Dacomitinib antagonizes multidrug resistance (MDR) in cancer cells by inhibiting the efflux activity of ABCB1 and ABCG2 transporters. *Cancer letters* **421**: 186-198.

Field JJ, Kanakkanthara A and Miller JH (2014) Microtubule-targeting agents are clinically successful due to both mitotic and interphase impairment of microtubule function. *Bioorganic & medicinal chemistry* **22**(18): 5050-5059.

Fojo T and Menefee M (2007) Mechanisms of multidrug resistance: the potential role of microtubule-stabilizing agents. *Annals of oncology : official journal of the European Society for Medical Oncology* **18 Suppl 5**: v3-8.

Frank NY, Margaryan A, Huang Y, Schatton T, Waaga-Gasser AM, Gasser M, Sayegh MH, Sadee W and Frank MH (2005) ABCB5-mediated doxorubicin transport and chemoresistance in human malignant melanoma. *Cancer research* **65**(10): 4320-4333.

Galmarini CM, Martin M, Bouchet BP, Guillen-Navarro MJ, Martinez-Diez M, Martinez-Leal JF, Akhmanova A and Aviles P (2018) Plocabulin, a novel tubulin-binding agent, inhibits angiogenesis by modulation of microtubule dynamics in endothelial cells. *BMC cancer* **18**(1): 164.

Gangjee A, Zaware N, Devambatla RK, Raghavan S, Westbrook CD, Dybdal-Hargreaves NF, Hamel E and Mooberry SL (2013) Synthesis of N(4)-(substituted phenyl)-N(4)-

alkyl/desalkyl-9H-pyrimido[4,5-b]indole-2,4-diamines and identification of new microtubule disrupting compounds that are effective against multidrug resistant cells. *Bioorganic & medicinal chemistry* **21**(4): 891-902.

Gangjee A, Zhao Y, Lin L, Raghavan S, Roberts EG, Risinger AL, Hamel E and Mooberry SL (2010) Synthesis and discovery of water-soluble microtubule targeting agents that bind to the colchicine site on tubulin and circumvent Pgp mediated resistance. *J Med Chem* **53**(22): 8116-8128.

Gigant B, Wang C, Ravelli RB, Roussi F, Steinmetz MO, Curmi PA, Sobel A and Knossow M (2005) Structural basis for the regulation of tubulin by vinblastine. *Nature* **435**(7041): 519-522.

Gillet JP, Calcagno AM, Varma S, Marino M, Green LJ, Vora MI, Patel C, Orina JN, Eliseeva TA, Singal V, Padmanabhan R, Davidson B, Ganapathi R, Sood AK, Rueda BR, Ambudkar SV and Gottesman MM (2011) Redefining the relevance of established cancer cell lines to the study of mechanisms of clinical anti-cancer drug resistance. *Proceedings of the National Academy of Sciences of the United States of America* **108**(46): 18708-18713.

Gottesman MM, Fojo T and Bates SE (2002) Multidrug resistance in cancer: role of ATP-dependent transporters. *Nature reviews Cancer* **2**(1): 48-58.

Hari M, Yang H, Zeng C, Canizales M and Cabral F (2003) Expression of class III beta-tubulin reduces microtubule assembly and confers resistance to paclitaxel. *Cell motility and the cytoskeleton* **56**(1): 45-56.

Hodges LM, Markova SM, Chinn LW, Gow JM, Kroetz DL, Klein TE and Altman RB (2011) Very important pharmacogene summary: ABCB1 (MDR1, P-glycoprotein). *Pharmacogenetics and Genomics* **21**(3): 152-161.

Homolya L, Orban TI, Csanady L and Sarkadi B (2011) Mitoxantrone is expelled by the ABCG2 multidrug transporter directly from the plasma membrane. *Biochim Biophys Acta* **1808**(1): 154-163.

Hwang DJ, Wang J, Li W and Miller DD (2015) Structural Optimization of Indole Derivatives Acting at Colchicine Binding Site as Potential Anticancer Agents. *ACS medicinal chemistry letters* **6**(9): 993-997.

Ji YT, Liu YN and Liu ZP (2015) Tubulin colchicine binding site inhibitors as vascular disrupting agents in clinical developments. *Current medicinal chemistry* **22**(11): 1348-1360.

Jordan MA (2002) Mechanism of action of antitumor drugs that interact with microtubules and tubulin. *Current medicinal chemistry Anti-cancer agents* **2**(1): 1-17.

Kalal BS, Upadhya D and Pai VR (2017) Chemotherapy Resistance Mechanisms in Advanced Skin Cancer. *Oncology reviews* **11**(1): 326.

Kamath K, Wilson L, Cabral F and Jordan MA (2005) BetaIII-tubulin induces paclitaxel resistance in association with reduced effects on microtubule dynamic instability. *The Journal of biological chemistry* **280**(13): 12902-12907.

Kanakkanthara A, Eras J, Northcote PT, Cabral F and Miller JH (2014) Resistance to peloruside A and laulimalide: functional significance of acquired betaI-tubulin mutations at sites important for drug-tubulin binding. *Curr Cancer Drug Targets* **14**(1): 79-90.

Kavallaris M (2010) Microtubules and resistance to tubulin-binding agents. *Nature reviews Cancer* **10**(3): 194-204.

Kline-Smith SL and Walczak CE (2004) Mitotic spindle assembly and chromosome segregation: refocusing on microtubule dynamics. *Molecular cell* **15**(3): 317-327.

Li W, Sun H, Xu S, Zhu Z and Xu J (2017a) Tubulin inhibitors targeting the colchicine binding site: a perspective of privileged structures. *Future medicinal chemistry* **9**(15): 1765-1794.

Li W, Sun H, Xu S, Zhu Z and Xu J (2017b) Tubulin inhibitors targeting the colchicine binding site: a perspective of privileged structures. *Future medicinal chemistry* **9**(15): 1765-1794.

Linos E, Swetter SM, Cockburn MG, Colditz GA and Clarke CA (2009) Increasing burden of melanoma in the United States. *The Journal of investigative dermatology* **129**(7): 1666-1674.

Loong HH and Yeo W (2014) Microtubule-targeting agents in oncology and therapeutic potential in hepatocellular carcinoma. *OncoTargets and therapy* **7**: 575-585.

Lu Y, Chen J, Xiao M, Li W and Miller DD (2012) An overview of tubulin inhibitors that interact with the colchicine binding site. *Pharmaceutical research* **29**(11): 2943-2971.

Lu Y, Li CM, Wang Z, Chen J, Mohler ML, Li W, Dalton JT and Miller DD (2011) Design, synthesis, and SAR studies of 4-substituted methoxylbenzoyl-aryl-thiazoles analogues as potent and orally bioavailable anticancer agents. *J Med Chem* **54**(13): 4678-4693.

Luo Y, Ellis LZ, Dallaglio K, Takeda M, Robinson WA, Robinson SE, Liu W, Lewis KD, McCarter MD, Gonzalez R, Norris DA, Roop DR, Spritz RA, Ahn NG and Fujita M (2012) Side population cells from human melanoma tumors reveal diverse mechanisms for chemoresistance. *The Journal of investigative dermatology* **132**(10): 2440-2450.

Martel-Frachet V, Keramidas M, Nurisso A, DeBonis S, Rome C, Coll JL, Boumendjel A, Skoufias DA and Ronot X (2015) IPP51, a chalcone acting as a microtubule inhibitor with in vivo antitumor activity against bladder carcinoma. *Oncotarget* **6**(16): 14669-14686.

Matter A (2001) Tumor angiogenesis as a therapeutic target. *Drug Discovery Today* **6**(19): 1005-1024.

McCoy AJ, Grosse-Kunstleve RW, Adams PD, Winn MD, Storoni LC and Read RJ (2007) Phaser crystallographic software. *Journal of applied crystallography* **40**(Pt 4): 658-674.

Mhaidat NM, Thorne RF, de Bock CE, Zhang XD and Hersey P (2008) Melanoma cell sensitivity to Docetaxel-induced apoptosis is determined by class III β-tubulin levels. *FEBS Letters* **582**(2): 267-272.

Mitchison T and Kirschner M (1984) Dynamic instability of microtubule growth. *Nature* **312**(5991): 237-242.

Morris PG and Fornier MN (2008) Microtubule active agents: beyond the taxane frontier. *Clinical cancer research : an official journal of the American Association for Cancer Research* **14**(22): 7167-7172.

Mukhtar E, Adhami VM and Mukhtar H (2014) Targeting microtubules by natural agents for cancer therapy. *Molecular cancer therapeutics* **13**(2): 275-284.

Orr GA, Verdier-Pinard P, McDaid H and Horwitz SB (2003) Mechanisms of Taxol resistance related to microtubules. *Oncogene* **22**(47): 7280-7295.

Otwinowski Z and Minor W (1997) [20] Processing of X-ray diffraction data collected in oscillation mode. *Methods in enzymology* **276**: 307-326.

Pasquier E and Kavallaris M (2008) Microtubules: a dynamic target in cancer therapy. *IUBMB life* **60**(3): 165-170.

Patel A, Li T-W, Anreddy N, Wang D-S, Sodani K, Gadhia S, Kathawala R, Yang D-H, Cheng C and Chen Z-S (2017) Suppression of ABCG2 mediated MDR in vitro and in vivo by a novel inhibitor of ABCG2 drug transport. *Pharmacological research* **121**: 184-193.

Perez EA (2009a) Microtubule inhibitors: Differentiating tubulin-inhibiting agents based on mechanisms of action, clinical activity, and resistance. *Molecular cancer therapeutics*: 1535-7163. MCT-1509-0366.

Perez EA (2009b) Microtubule inhibitors: Differentiating tubulin-inhibiting agents based on mechanisms of action, clinical activity, and resistance. *Mol Cancer Ther* **8**(8): 2086-2095.

Prota AE, Bargsten K, Zurwerra D, Field JJ, Diaz JF, Altmann KH and Steinmetz MO (2013) Molecular mechanism of action of microtubule-stabilizing anticancer agents. *Science (New York, NY)* **339**(6119): 587-590.

Rai A, Surolia A and Panda D (2012) An antitubulin agent BCFMT inhibits proliferation of cancer cells and induces cell death by inhibiting microtubule dynamics. *PloS one* **7**(8): e44311.

Ranganathan S, Benetatos CA, Colarusso PJ, Dexter DW and Hudes GR (1998) Altered beta-tubulin isotype expression in paclitaxel-resistant human prostate carcinoma cells. *British journal of cancer* **77**(4): 562-566.

Ravelli RB, Gigant B, Curmi PA, Jourdain I, Lachkar S, Sobel A and Knossow M (2004) Insight into tubulin regulation from a complex with colchicine and a stathmin-like domain. *Nature* **428**(6979): 198-202.

Robey RW, Honjo Y, van de Laar A, Miyake K, Regis JT, Litman T and Bates SE (2001) A functional assay for detection of the mitoxantrone resistance protein, MXR (ABCG2). *Biochimica et Biophysica Acta (BBA)-Biomembranes* **1512**(2): 171-182.

Rohena CC, Telang NS, Da C, Risinger AL, Sikorski JA, Kellogg GE, Gupton JT and Mooberry SL (2016) Biological Characterization of an Improved Pyrrole-Based Colchicine Site Agent Identified through Structure-Based Design. *Molecular pharmacology* **89**(2): 287-296.

Sakchaisri K, Kim SO, Hwang J, Soung NK, Lee KH, Choi TW, Lee Y, Park CM, Thimmegowda NR, Lee PY, Shwetha B, Srinivasrao G, Pham TT, Jang JH, Yum HW, Surh YJ, Lee KS, Park H, Kim SJ, Kwon YT, Ahn JS and Kim BY (2017) Anticancer activity of a novel small molecule tubulin inhibitor STK899704. *PloS one* **12**(3): e0173311.

Schadendorf D, Herfordt R and Czarnetzki BM (1995) P-glycoprotein expression in primary and metastatic malignant melanoma. *The British journal of dermatology* **132**(4): 551-555.

Schmidt M and Bastians H (2007) Mitotic drug targets and the development of novel anti-mitotic anticancer drugs. *Drug Resist Updat* **10**(4-5): 162-181.

Schwartz EL (2009) Antivascular actions of microtubule-binding drugs. *Clinical cancer research : an official journal of the American Association for Cancer Research* **15**(8): 2594-2601.

Stanton RA, Gernert KM, Nettles JH and Aneja R (2011) Drugs that target dynamic microtubules: a new molecular perspective. *Medicinal research reviews* **31**(3): 443-481.

Stengel C, Newman SP, Leese MP, Potter BV, Reed MJ and Purohit A (2010) Class III beta-tubulin expression and in vitro resistance to microtubule targeting agents. *British journal of cancer* **102**(2): 316-324.

Su M, Huang J, Liu S, Xiao Y, Qin X, Liu J, Pi C, Luo T, Li J, Chen X and Luo Z (2016) The anti-angiogenic effect and novel mechanisms of action of Combretastatin A-4. *Sci Rep* **6**: 28139.

Szakacs G, Paterson JK, Ludwig JA, Booth-Genthe C and Gottesman MM (2006) Targeting multidrug resistance in cancer. *Nature reviews Drug discovery* **5**(3): 219-234.

Vlaming ML, Lagas JS and Schinkel AH (2009) Physiological and pharmacological roles of ABCG2 (BCRP): recent findings in Abcg2 knockout mice. *Advanced drug delivery reviews* **61**(1): 14-25.

Wang B, Ma L-Y, Wang J-Q, Lei Z-N, Gupta P, Zhao Y-D, Li Z-H, Liu Y, Zhang X-H and Li Y-N (2018) Discovery of 5-cyano-6-phenylpyrimidin derivatives containing an acylurea moiety as orally bioavailable reversal agents against P-glycoprotein-mediated mutidrug resistance. *Journal of medicinal chemistry* **61**(14): 5988-6001.

Wang J, Chen J, Miller DD and Li W (2014) Synergistic combination of novel tubulin inhibitor ABI-274 and vemurafenib overcome vemurafenib acquired resistance in BRAFV600E melanoma. *Mol Cancer Ther* **13**(1): 16-26.

Wang Y, Yu Y, Li GB, Li SA, Wu C, Gigant B, Qin W, Chen H, Wu Y, Chen Q and Yang J (2017a) Mechanism of microtubule stabilization by taccalonolide AJ. *Nature communications* **8**: 15787.

Wang Y, Zhang H, Gigant B, Yu Y, Wu Y, Chen X, Lai Q, Yang Z, Chen Q and Yang J (2016) Structures of a diverse set of colchicine binding site inhibitors in complex with tubulin provide a rationale for drug discovery. *The FEBS journal* **283**(1): 102-111.

Wang YJ, Zhang YK, Zhang GN, Al Rihani SB, Wei MN, Gupta P, Zhang XY, Shukla S, Ambudkar SV, Kaddoumi A, Shi Z and Chen ZS (2017b) Regorafenib overcomes chemotherapeutic multidrug resistance mediated by ABCB1 transporter in colorectal cancer: In vitro and in vivo study. *Cancer Lett* **396**: 145-154.

Wang Z, Chen J, Wang J, Ahn S, Li CM, Lu Y, Loveless VS, Dalton JT, Miller DD and Li W (2012) Novel tubulin polymerization inhibitors overcome multidrug resistance and reduce melanoma lung metastasis. *Pharmaceutical research* **29**(11): 3040-3052.

Weiderhold KN, Randall-Hlubek DA, Polin LA, Hamel E and Mooberry SL (2006) CB694, a novel antimitotic with antitumor activities. *International journal of cancer* **118**(4): 1032-1040.

Wu CP, Hsieh CH and Wu YS (2011) The emergence of drug transporter-mediated multidrug resistance to cancer chemotherapy. *Molecular pharmaceutics* **8**(6): 1996-2011.

Wu S and Singh RK (2011) Resistance to chemotherapy and molecularly targeted therapies: rationale for combination therapy in malignant melanoma. *Current molecular medicine* **11**(7): 553-563.

Wu X, Wang Q and Li W (2016) Recent Advances in Heterocyclic Tubulin Inhibitors Targeting the Colchicine Binding Site. *Anti-cancer agents in medicinal chemistry* **16**(10): 1325-1338.

Xia CQ and Smith PG (2012) Drug efflux transporters and multidrug resistance in acute leukemia: therapeutic impact and novel approaches to mediation. *Molecular pharmacology* **82**(6): 1008-1021.

Yusuf RZ, Duan Z, Lamendola DE, Penson RT and Seiden MV (2003) Paclitaxel resistance: molecular mechanisms and pharmacologic manipulation. *Curr Cancer Drug Targets* **3**(1): 1-19.

Molecular Pharmacology Fast Forward. Published on May 1, 2019 as DOI: 10.1124/mol.118.114801
This article has not been copyedited and formatted. The final version may differ from this version.

FIGURES LEGENDS

Figure 1. DJ95 is potent against NCI-60 cell lines.

NCI DTP 5-dose assay mean graphs. Positive values indicate net cell growth, 0 represents no net growth, and negative values indicate cell lethality.

Figure 2. DJ95 inhibits cell proliferation and migration of melanoma.

A) Colony formation assay of A375 cells treated with DJ95 in 6 well plates (n=3). Cells were treated with indicated concentrations of DJ95 and media only was used as the control. (B) Quantification of colony area using ImageJ software. Graph is represented as area ± SD. (C) Representative images of A375 (top) and RPMI-7951 cells (bottom) in a wound healing assay (n=3). A scratch was created through a monolayer of confluent cells, which were then treated with DJ95 or control. The migrating ability was calculated from images taken at the start of the treatment and after 24 hr incubation with compound. The yellow outline represents the leading edge of the area boundary as determined by ImageJ software. (D) Quantification of A375 and (E) RPMI-7951 migration represented as a percentage of the initial scratch area ± SD. Statistical significance was determined by one-way ANOVA followed by Dunnett's multiple comparison test, comparing each treatment group to the control group for the above experiments. (**$p < 0.01$, ***$p < 0.001$, ****$p < 0.0001$).

Figure 3. DJ95 interferes with microtubule networks and mitotic spindle organization.

(A) Microtubule networks of WM-164 cells after 18 hr treatment with paclitaxel or DJ95 at indicated concentrations compared to untreated cells. The fragmentation and destabilization of the microtubules is evident from DJ95 treatment, whereas paclitaxel increased polymerization and stabilization. (B) The effect on mitotic spindle organization after 18 hr treatment with 100 and 200 nM concentrations of DJ95. Mitotic spindle suppression is evidenced by multiple asters

and disorganized spindle morphology. Confocal images were obtained from Keyence BZX microscope. Tubulin (red) is visualized by α-tubulin primary antibody and Alexa Fluor 647 secondary antibody and DNA (blue) is stained with DAPI.

Figure 4: The Crystal Structure of the T2R-TTL-DJ95 Complex.

(A) Quaternary structure of the T2R-TTL-DJ95 complex showing the arrangement of the protein components, the bound nucleotides and the bound DJ95. Note that DJ95 only occupies one of the available α/β-tubulin interfaces. (B) Close-up view of the bound DJ95 (yellow carbons) and its interactions with surrounding residues from β-tubulin (cyan). Note the hydrogen bond to the backbone carbonyl oxygen of α-tubulin Thr179 (green) across the α/β interface. (C) Close-up view of the superimposed DJ95 complex and the colchicine complex (PDB ID: 4O2B, grey). Note that DJ95 is slightly more extended than colchicine. (D) Close-up view of the 'curved' DJ95 complex superimposed on the 'straight' Taxol complex (PDB ID: 1JFF, wheat). The red arrows indicate the extent of movement of b-tubulin with respect to a-tubulin upon the binding of DJ95. Note that the binding of DJ95 is not compatible with the 'straight' complex.

Figure 5. Biacore surface plasmon resonance kinetic analyses of DJ95, colchicine, and CA-4 interacting with tubulin.

Binding kinetics of DJ95 (32, 16, 8, 4, 2 μM), Colchicine (20, 10, 5, 2.5, 1.25 μM), and CA-4 （20, 10, 5, 2.5, 1.25 μM) to tubulin (17,000 RU) determined by SPR technology. The calculated equilibrium dissociation constant Kd values for DJ95, colchicine and CA-4 is 59.4 μM, 5.7 μM, and 7.7 μM, respectively.

Molecular Pharmacology Fast Forward. Published on May 1, 2019 as DOI: 10.1124/mol.118.114801
This article has not been copyedited and formatted. The final version may differ from this version.

Figure 6. DJ95 in binding and enzyme and uptake assays.

(A) DJ95 control-specific binding as a % inhibition to the binding to a radioactively labeled ligand specific for each target. (B) DJ95 enzyme based functional a % of control enzyme activity. Results showing an inhibition or stimulation higher than 50% are considered to represent significant effects of the test compounds. Graphs are represented as the mean of duplicate assays ± SD. Screening was performed by Eurofins Cerep-Panlabs.

Figure 7. DJ95 inhibits melanoma tumor growth *in vivo*.

(A) Plasma concentrations at each timepoint following i.p. injection of DJ95 at 15 mg/kg concentration shown as individual replicates connected by mean (n=3 per time point). (B) A375 melanoma xenograft model in nude mice. Mice were dosed by i.p. injection 5 times a week for 2 weeks with vehicle solution only or 15 mg/kg DJ95. Mean tumor volume is expressed as % growth compared to tumor volume at the beginning of the experiment ± SEM (n=6 for treated group,7 for control). (C) Individual tumor volumes at the end of the experiment shown as mean ± SD. (D) Mouse weight change throughout the study shown as mean ± SD. (E) Resected tumor weight at the end of the experiment expressed as mean ± SD. Statistical significance was determined by student's t test comparing treatment group to the vehicle control group (*$p< 0.05$, **$p< 0.01$).

Figure 8. DJ95 targets tumor vascular and capillary network formation.

(A) Representative images of HUVEC capillary formation on matrigel. Images were taken after 6 hr incubation with indicated concentrations of DJ95 or colchicine. (B) Quantification of total tube length using Image J analysis expressed as mean ± SD (n=4). Statistical analysis was performed using one-way ANOVA comparing each group to the control. (C) Representative

Molecular Pharmacology Fast Forward. Published on May 1, 2019 as DOI: 10.1124/mol.118.114801
This article has not been copyedited and formatted. The final version may differ from this version.

immunohistochemistry images of CD31 stained tumor sections taken at 10x. (D) Positive stained area calculated for tumor sections at 20x magnification (5 images per tumor, 3 separate tumors per group) represented as mean pixels ± SD. Statistical significance was determined by a student's t test without correction for multiple comparisons. (**$p< 0.01$, ***$p< 0.001$, ****$p< 0.0001$).

Molecular Pharmacology Fast Forward. Published on May 1, 2019 as DOI: 10.1124/mol.118.114801
This article has not been copyedited and formatted. The final version may differ from this version.

TABLES

Table 1. Cytotoxic effects of DJ95 against malignant melanoma cancer cell lines.

Treatment	IC_{50} [a] ± SD (nM)				
	A375	RPMI-7951	WM-164	WM115	SK-MEL-1
DJ95	24.7 ± 4.9	58.9 ± 13.3	68.2 ± 12.4	99.8 ± 16.8	78.7 ± 16.5
Colchicine	10.6 ± 1.8	11.1 ± 0.7	10.1 ± 0.7	9.3 ± 1.0	11.5 ± 2.5
Paclitaxel	2.5 ± 1.0	3.4 ± 0.8	8.0 ± 1.0	3.3 ± 1.6	1.8 ± 0.8

[a] IC_{50} values represent the mean ± SD of three independent experiments performed in quadruplicate.

Molecular Pharmacology Fast Forward. Published on May 1, 2019 as DOI: 10.1124/mol.118.114801
This article has not been copyedited and formatted. The final version may differ from this version.

Table 2. Cytotoxic effects of DJ95 against parental and gene transfected ABCB1-, ABCC1- or ABCG2-overexpressing cancer cell lines.

Treatment	IC_{50}[b] ± SD (nM)			
	HEK293/pcDNA3.1	HEK293/ABCB1	HEK293/ABCC1	HEK293/ABCG2-R482
DJ95	330.0 ± 44.1	314.7 ± 73.1	1213.9 ± 241.6	2869.2 ± 123.3
Paclitaxel	34.6 ± 6.3	3496.0 ± 657.8	>10000	>10000
Colchicine	112.1 ± 41.5	>10000	>10000	>10000
Vincristine	99.4 ± 23.1	>10000	>10000	>10000
Mitoxantrone	108.0 ± 27.5	—	—	1209.7 ± 111.4
Cisplatin	2510.1 ± 362.6	2583.1 ± 474.5	2584.1 ± 151.8	2475.3 ± 127.4

[b] IC_{50} values represent the mean ± SD of three independent experiments performed in triplicate.

Molecular Pharmacology Fast Forward. Published on May 1, 2019 as DOI: 10.1124/mol.118.114801
This article has not been copyedited and formatted. The final version may differ from this version.

Table 3. Cytotoxic effects of DJ95 against parental and drug-selected ABCB1-, ABCC1- or ABCG2-overexpressing cancer cell lines.

Treatment	IC_{50}[b] ± SD (nM)				
	KB-3-1	KB-C2 (ABCB1)	KB-CV60 (ABCC1)	NCI-H460	NCI-H460/MX20 (ABCG2)
DJ95	23.5 ± 2.2	719.5 ± 181.5	35.9 ± 4.5	673.0 ± 111.7	5361.5 ± 645.5
Paclitaxel	9.2 ± 2.1	1918.5 ± 106.3	120.0 ± 14.6	>10000	>10000
Colchicine	23.9 ± 4.9	7445.3 ± 446.3	91.7 ± 7.7	>10000	>10000
Vincristine	1.3 ± 0.2	748.8 ± 99.8	218.6 ± 1.9	>10000	>10000
Mitoxantrone	—	—	—	118.7 ± 40.2	2456.5 ± 420.4
Cisplatin	2024.5 ± 463.7	2871.2 ± 115.3	1796.5 ± 198.8	2226.6 ± 179.5	2870.6 ± 281.7

[b] IC_{50} values represent the mean ± SD of three independent experiments performed in triplicate.

Molecular Pharmacology Fast Forward. Published on May 1, 2019 as DOI: 10.1124/mol.118.114801
This article has not been copyedited and formatted. The final version may differ from this version.

Table 4. X-ray data collection and refinement statistics. Tubulin-RB3_SLD-TTL complex bound with DJ95 (PDB ID: 6NNG). Values in parentheses are for highest-resolution shell.

Data collection	
Space group	$P2_12_12_1$
Cell dimensions	
a, *b*, *c* (Å)	105.42 157.98 182.84
α, β, γ (°)	90 90 90
Resolution (Å)	50 - 2.4 (2.44 - 2.4)
$R_{meas,}$	0.092 (0.922)
$I/\sigma(I)$	20.89 (2.14)
Completeness (%)	99.2 (99.5)
Redundancy	6.6 (6.4)
Refinement	
Resolution (Å)	48.25 - 2.4 (2.48 - 2.4)
No. reflections	117909 (10915)
R_{work} / R_{free}	0.1866 / 0.2253
No. atoms	17724
Protein	16956
Ligand/ion	215
Water	553
B factors	
Protein	49.92
Ligand/ion	52.57
Water	43.07
R.m.s. deviations	
Bond lengths (Å)	0.008
Bond angles (°)	1.05
Ramachandran Plot	
Favored (%)	98.04
Allowed (%)	1.91
Outliers (%)	0.05

Molecular Pharmacology Fast Forward. Published on May 1, 2019 as DOI: 10.1124/mol.118.114801
This article has not been copyedited and formatted. The final version may differ from this version.

FIGURES

Figure 1.

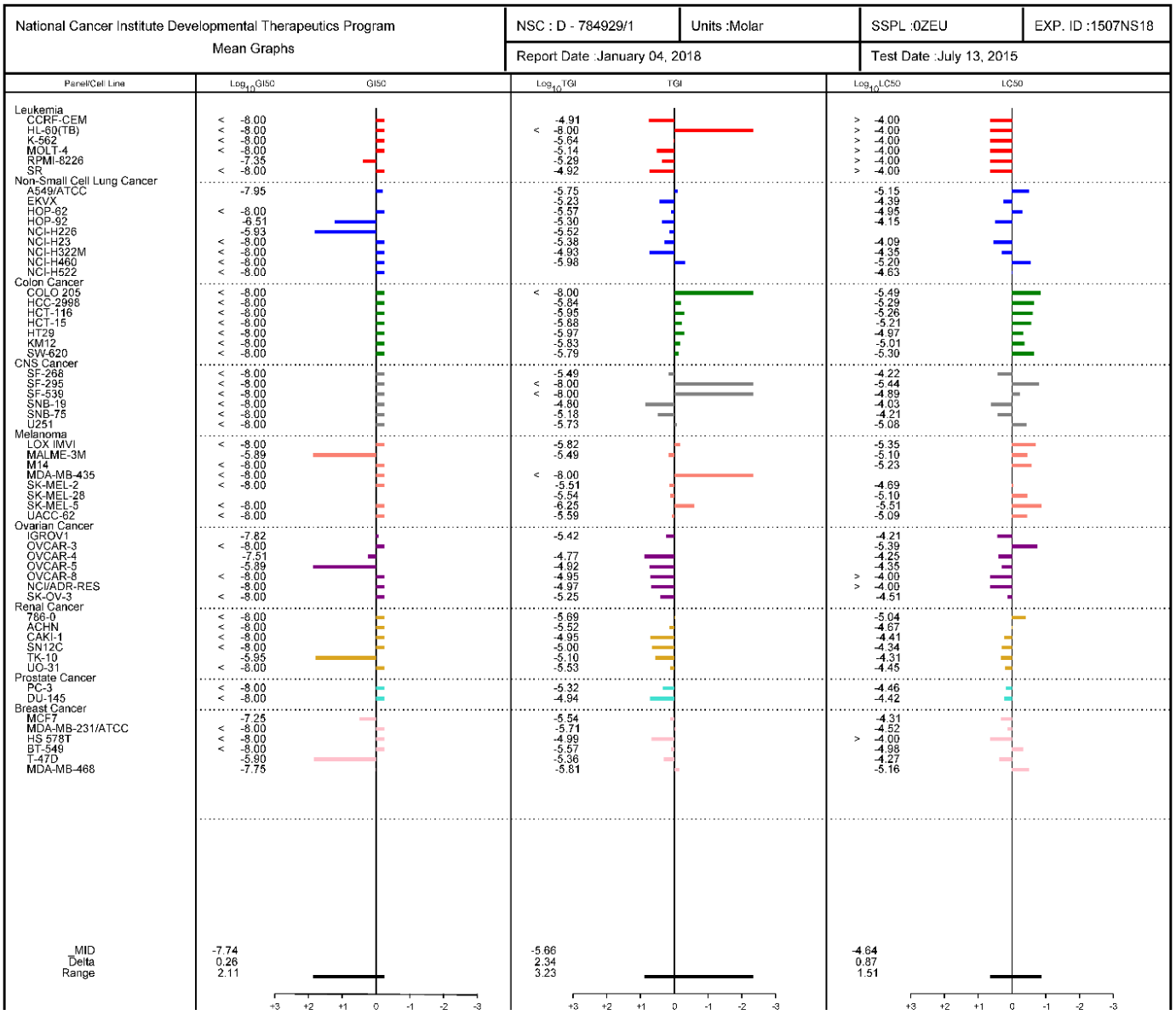

Molecular Pharmacology Fast Forward. Published on May 1, 2019 as DOI: 10.1124/mol.118.114801
This article has not been copyedited and formatted. The final version may differ from this version.

Figure 2.

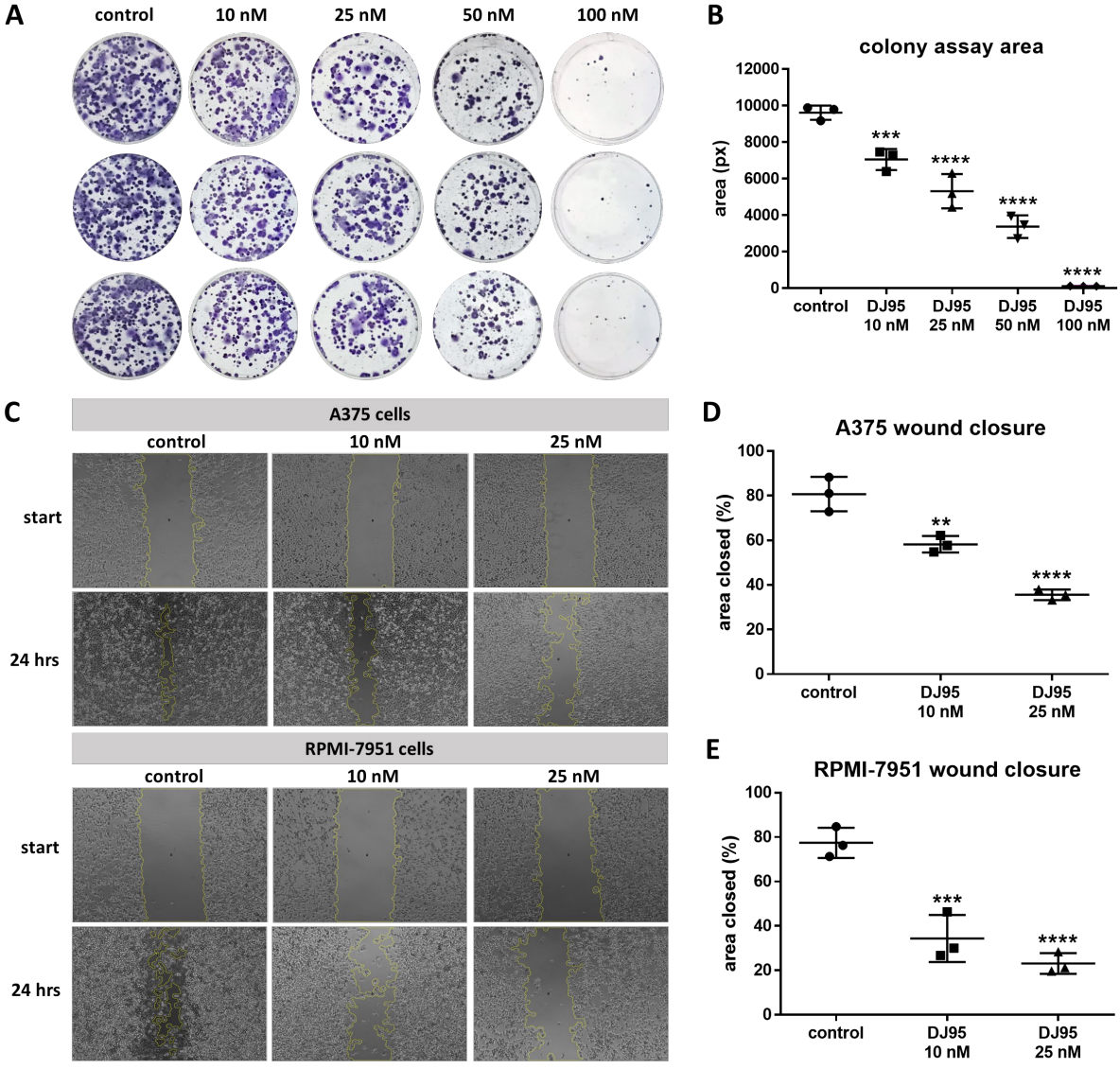

Molecular Pharmacology Fast Forward. Published on May 1, 2019 as DOI: 10.1124/mol.118.114801
This article has not been copyedited and formatted. The final version may differ from this version.

Figure 3.

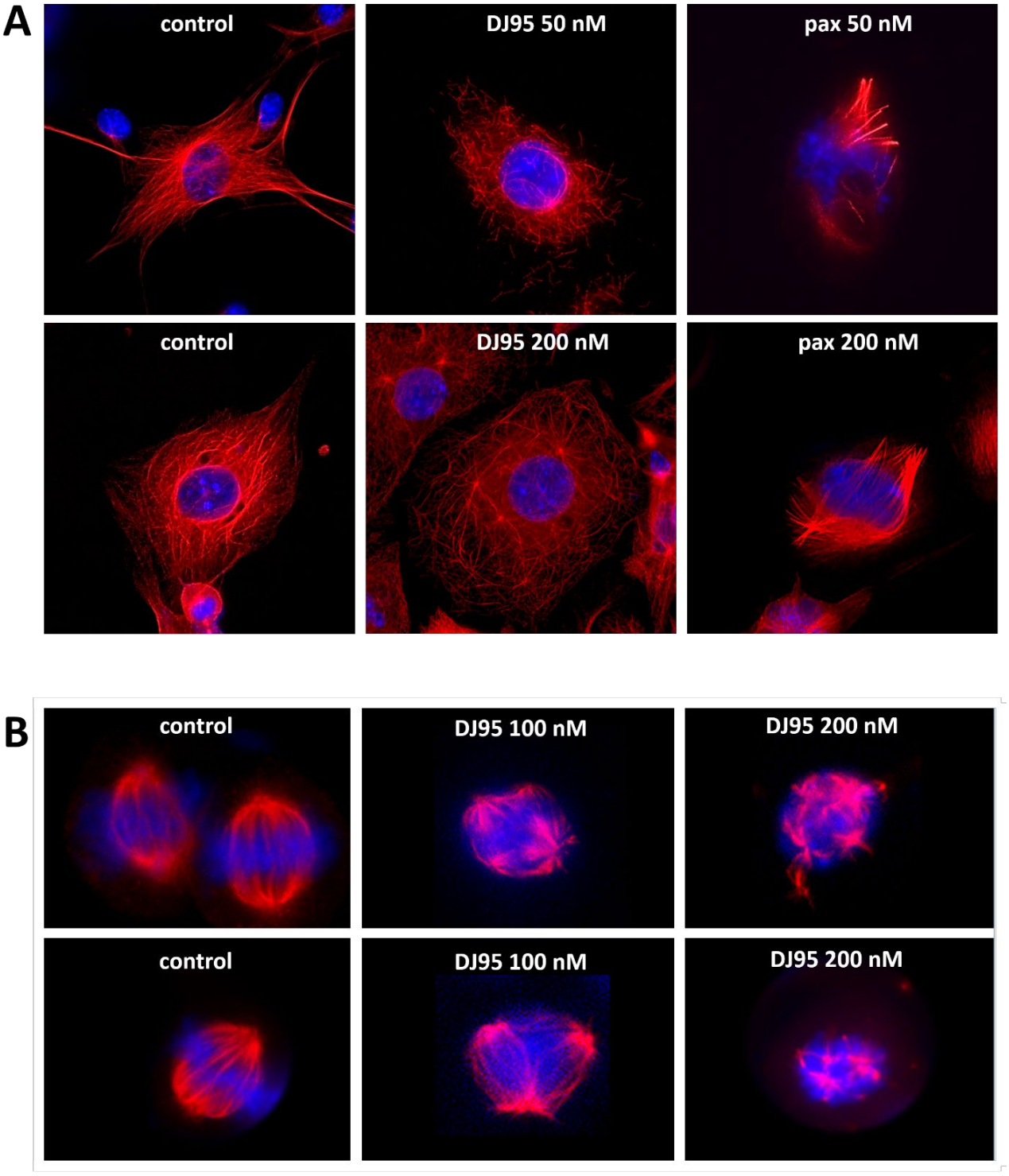

Molecular Pharmacology Fast Forward. Published on May 1, 2019 as DOI: 10.1124/mol.118.114801
This article has not been copyedited and formatted. The final version may differ from this version.

Figure 4.

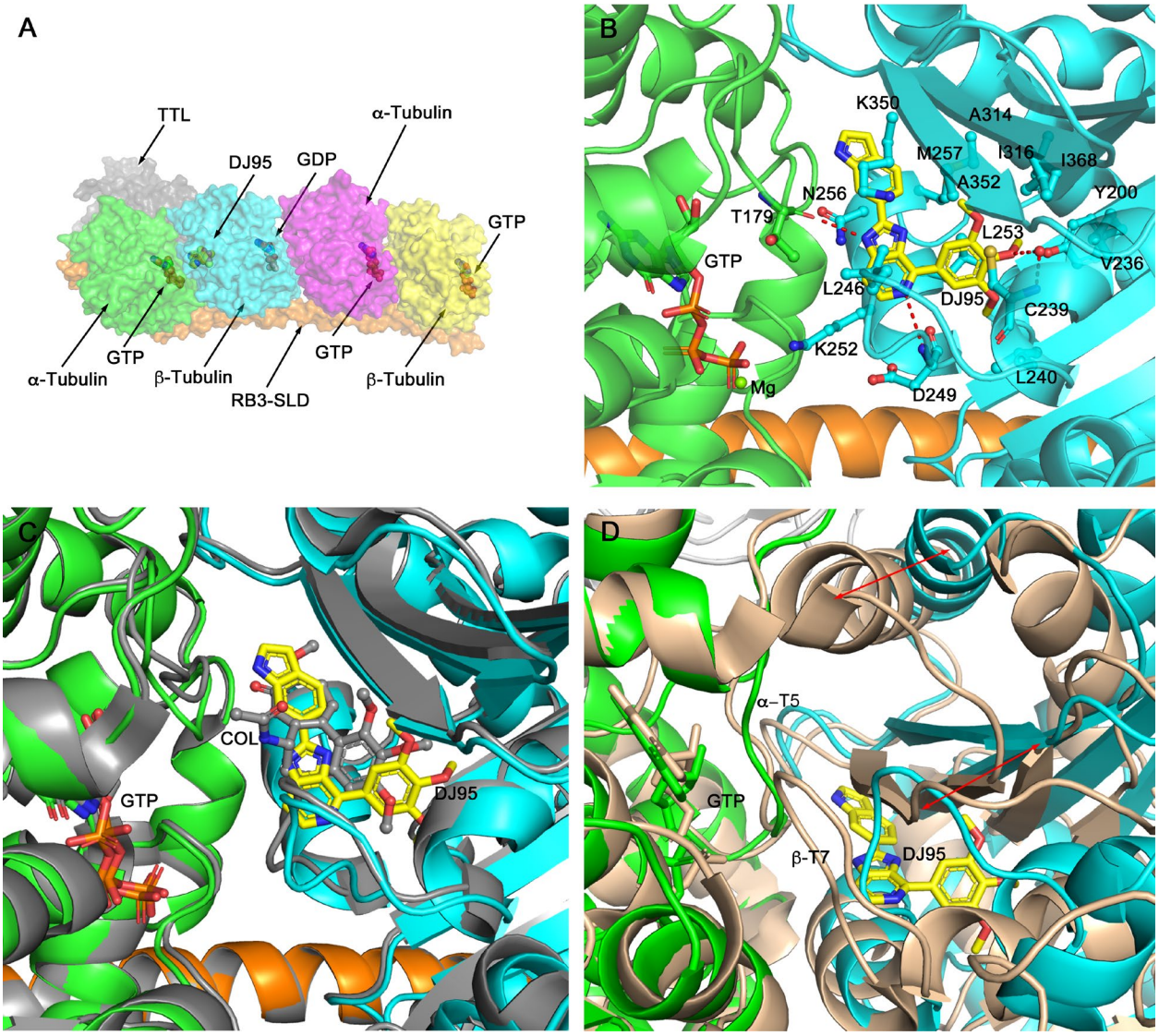

Molecular Pharmacology Fast Forward. Published on May 1, 2019 as DOI: 10.1124/mol.118.114801
This article has not been copyedited and formatted. The final version may differ from this version.

Figure 5.

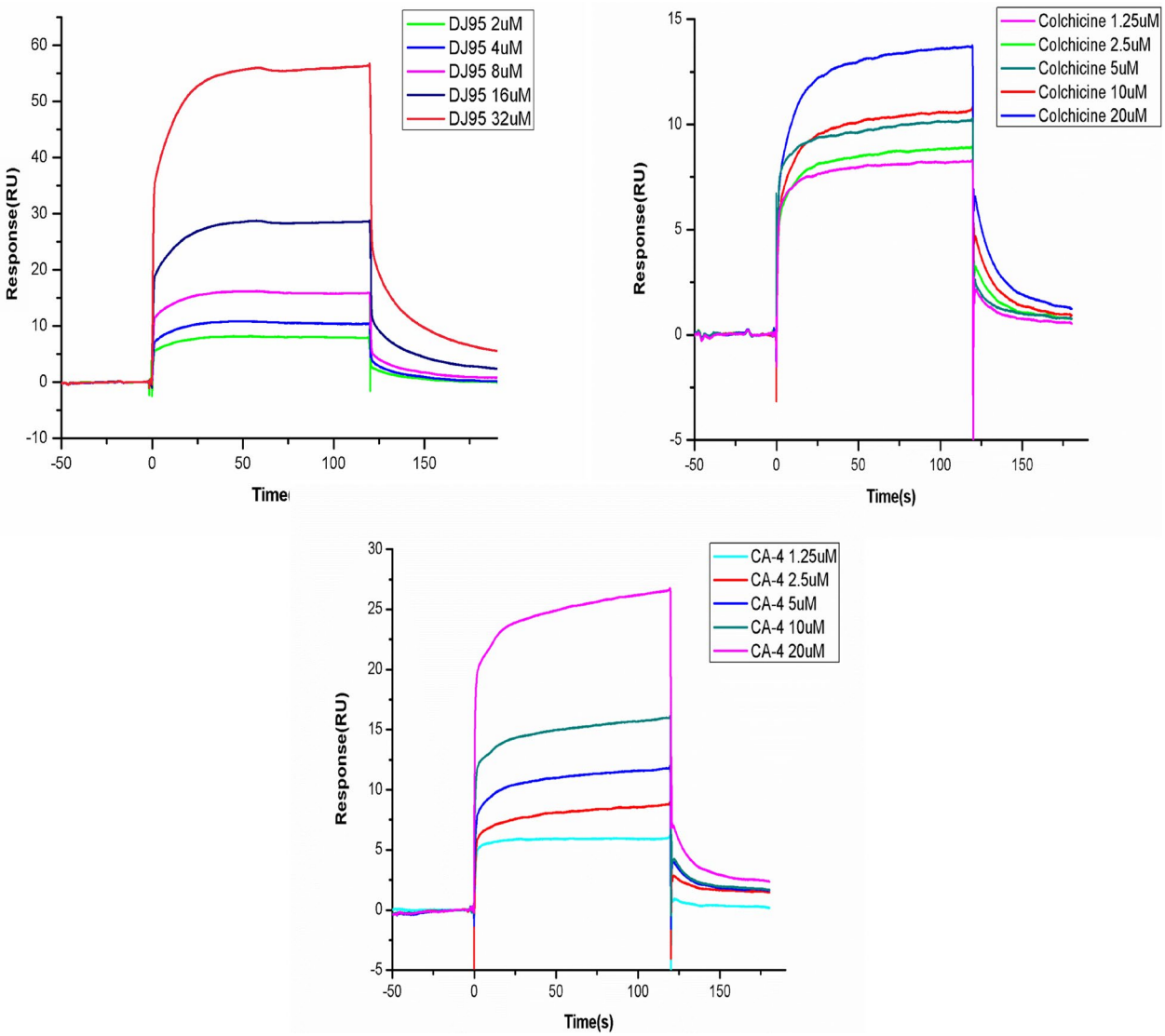

Molecular Pharmacology Fast Forward. Published on May 1, 2019 as DOI: 10.1124/mol.118.114801
This article has not been copyedited and formatted. The final version may differ from this version.

Figure 6.

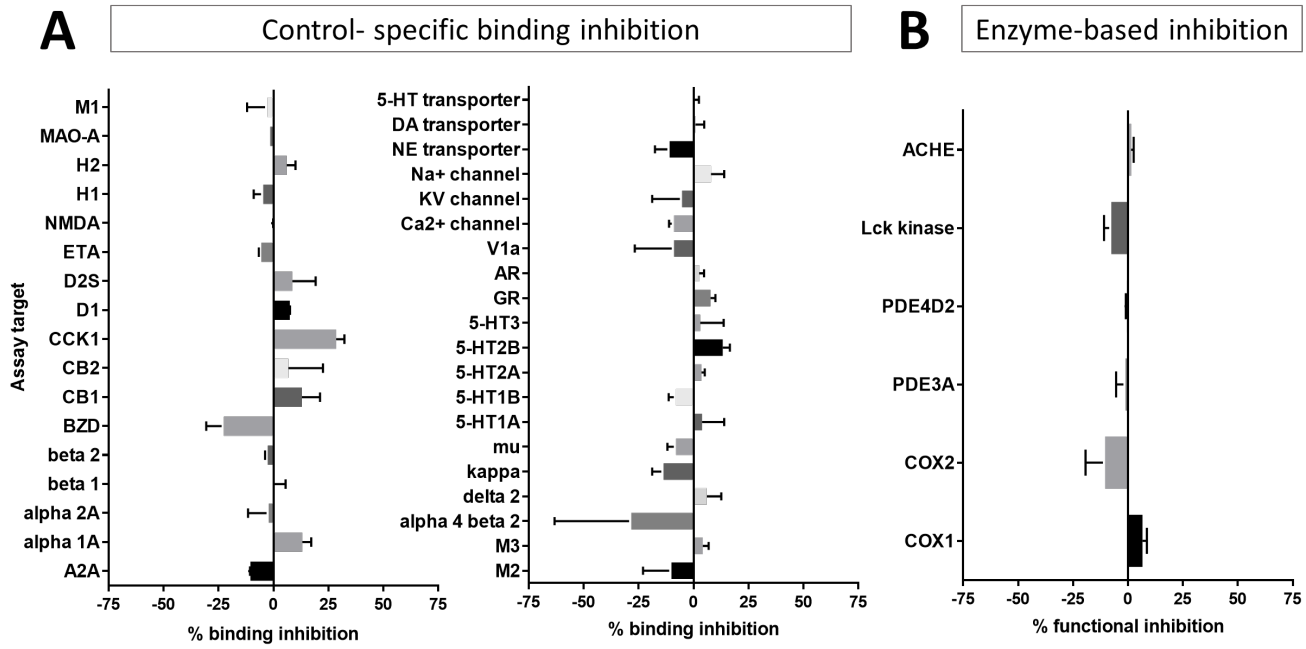

Molecular Pharmacology Fast Forward. Published on May 1, 2019 as DOI: 10.1124/mol.118.114801
This article has not been copyedited and formatted. The final version may differ from this version.

Figure 7.

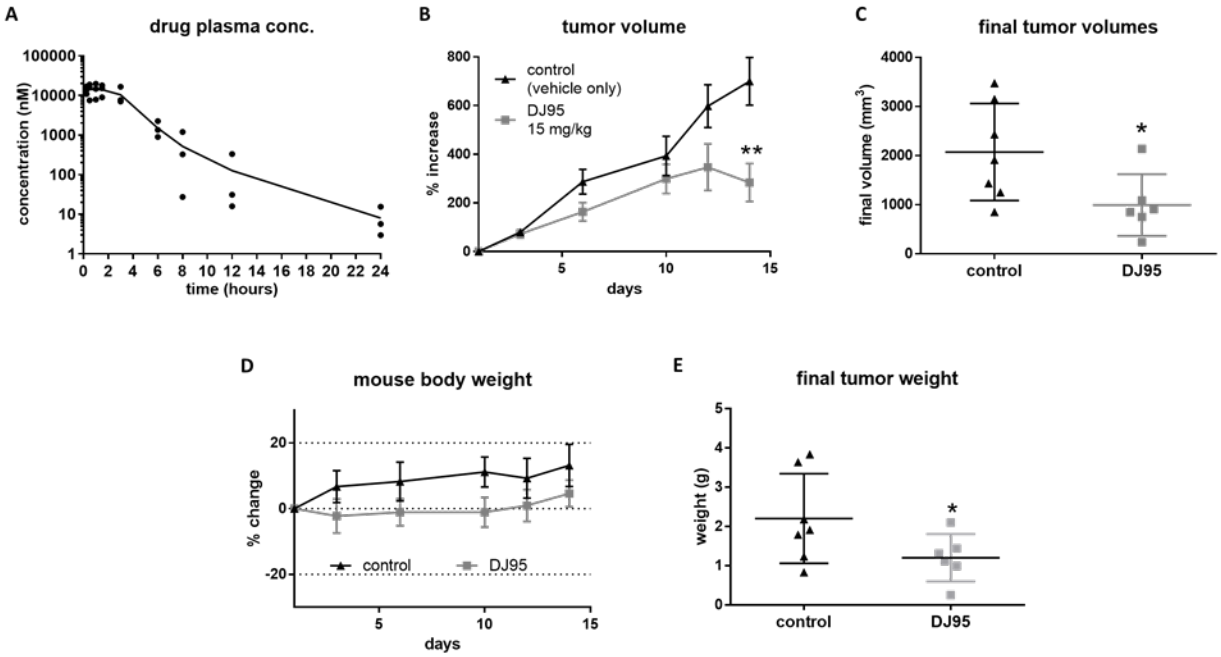

Molecular Pharmacology Fast Forward. Published on May 1, 2019 as DOI: 10.1124/mol.118.114801
This article has not been copyedited and formatted. The final version may differ from this version.

Figure 8.

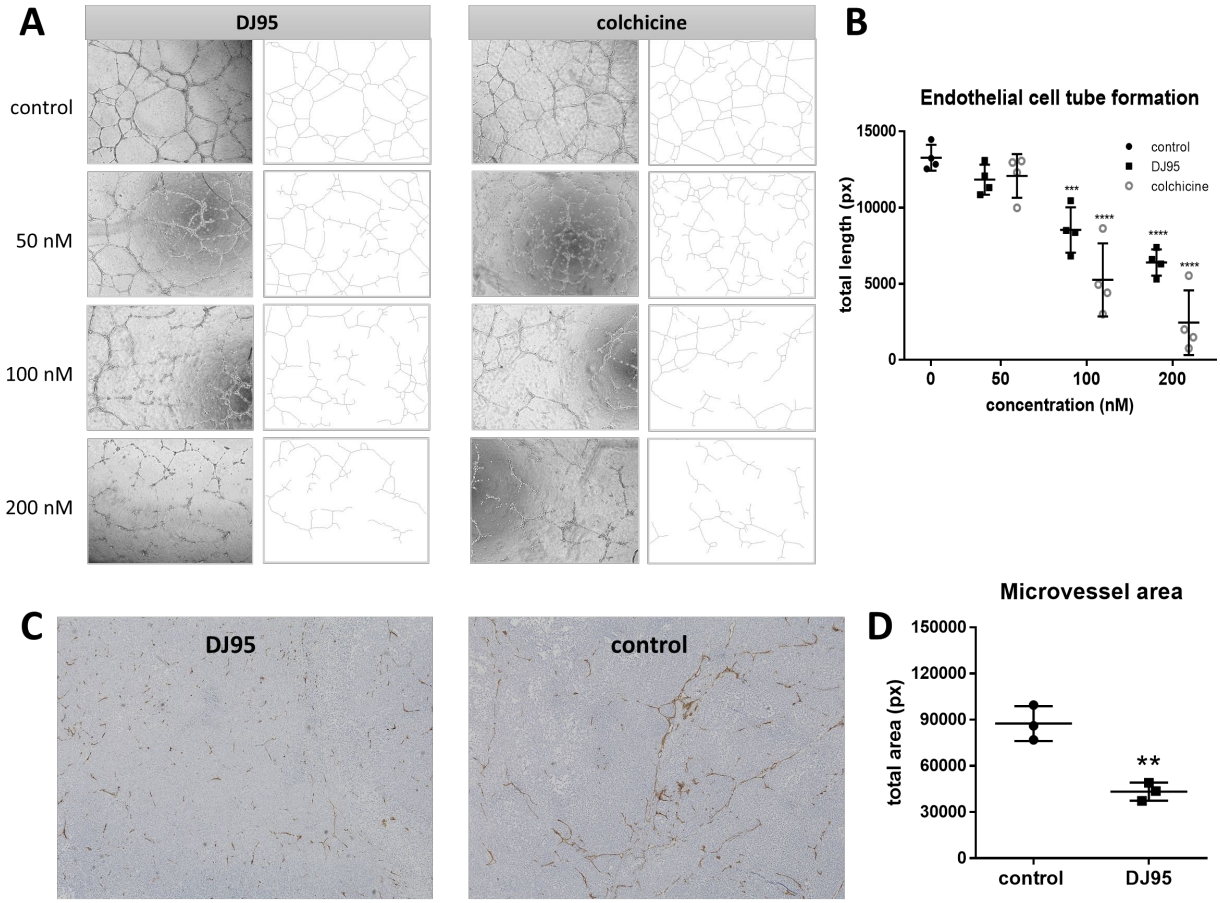

Supporting information

Colchicine binding site agent DJ95 overcomes drug resistance and exhibits antitumor efficacy

Authors: Kinsie E. Arnst[1], Yuxi Wang[2,3], Zi-Ning Lei[4], Dong-Jin Hwang[1], Gyanendra Kumar[5], Dejian Ma[1], Deanna N. Parke[6], Qiang Chen[2], Jinliang Yang[2], Stephen W. White[5], Tiffany N. Seagroves[6], Zhe-Sheng Chen[4], Duane D. Miller*[1], and Wei Li*[1]

Affiliation: [1]Department of Pharmaceutical Sciences, College of Pharmacy, the University of Tennessee Health Science Center, Memphis, TN. [2]State Key Laboratory of Biotherapy and Cancer Center, Collaborative Innovation Center of Biotherapy, [3] Department of Respiratory Medicine, West China Hospital, Sichuan University, Chengdu, China. [4]Department of Pharmaceutical Sciences, College of Pharmacy and Health Sciences, St. John's University, Queens, NY. [5] Department of Structural Biology, St. Jude Children's Research Hospital, Memphis, TN. [6]Department of Pathology, the University of Tennessee Health Science Center, Memphis, TN.

Supplement Table 1. Multiple reaction-monitoring (MRM) parameters based compound optimization.

Analyte	Transition (m/z)	T_R(min)	DP (V)	CE (V)	CXP (V)
DJ95	400.7/340.3	5.38	196	39	22
ABI-231 (IS)	378.3/210.2	5.10	186	37	12

T_R Retention time; DP, declustering potential; CE, collision energy; CXP, collision cell exit potential; IS internal standard

Supplement Table 2. Melanoma cell lines contain genomic mutations in the following genes according to the Sanger COSMIC database: BRAF, CKD4, CTNNB1, CDKN2A, NRAS, PTEN, TP53, and PPP6C.

Cell line	site	Reported gene mutations
A375	primary	BRAF, CDKN2A, PPP6C
RPMI-7951	metastatic	BRAF, CDKN2A, PTEN, TP53
WM-164	metastatic	BRAF, CDKN2A, TP53,
WM-115	primary	BRAF, NRAS, CDKN2A, PTEN,
SK-MEL-1	primary	BRAF, CDK4, CTNNB1, PPP6C

http://cancer.sanger.ac.uk

Supplement Table 3. Cytotoxic activities of DJ95 against NCI60 human cancer cell lines. GI_{50}, TGI, and LC_{50} values were obtained from the NCI-DTP five-dose assay and the mean growth % was obtained from the one-dose assay.

PANEL/CELL LINE	GI_{50} (NM)	TGI (μM)	LC_{50} (μM)	MEAN GROWTH %
Leukemia				
CCRF-CEM	<10.0	12.3	>100.0	5.3
HL-60(TB)	<10.0	<0.01	>100.0	-48.7
K-562	<10.0	2.3	>100.0	-14.4
MOLT-4	<10.0	7.2	>100.0	18.5
RPMI-8226	44.7	5.1	>100.0	-43.0
SR	<10.0	12.0	>100.0	-4.9
NSCLC				
A549/ATCC	11.2	1.8	7.1	-28.5
EKVX		5.9	40.7	30.9
HOP-62	<10.0	2.7	11.2	-19.6
HOP-92	309.0	5.0	70.8	-8.6
NCI-H226	1174.9	3.0	>100.0	19.3
NCI-H23	<10.0	4.2	81.3	26.1
NCI-H322M	<10.0	11.7	44.7	45.0
NCI-460	<10.0	1.0	6.3	2.6
NCI-H522	<10.0		23.4	-59.5
Colon cancer				
COLO 205	<10.0	<0.01	3.2	-71.5
HCC-2998	<10.0	1.4	5.1	-19.2
HCT-116	<10.0	1.1	5.5	4.4
HCT-15	<10.0	1.3	6.2	-7.0
HT29	<10.0	1.1	10.7	-37.8
KM12	<10.0	1.5	9.8	3.6
SW-620	<10.0	1.6	5.0	-15.6
CNS cancer				
SF-268	<10.0	3.2	60.3	19.3
SF-295	<10.0	<0.01	3.6	-59.4
SF-539	<10.0	<0.01	12.9	-19.5
SNB-19	<10.0	15.8	93.3	34.8
SNB-75	<10.0	6.6	61.7	18.9
U251	<10.0	1.9	8.3	-16.3
Melanoma				
LOX IMVI	<10.0	1.5	4.5	-67.5
MALME-3M	1288.2	3.2	7.9	21.7
M14	<10.0		5.9	4.3
MDA-MB-435	<10.0	<0.01	>100	5.2
SK-MEL-2	<10.0	3.1	20.4	15.2
SK-MEL-28		2.9	7.9	42.1
SK-MEL-5	<10.0	0.6	3.1	-38.4
UACC-62	<10.0	2.6	8.1	27.4

Supplement Table 3 continued

Panel/Cell line	GI_{50} (nM)	TGI (μM)	LC_{50} (μM)	mean growth %
Ovarian cancer				
IGROV1	15.1	3.8	61.7	29.5
OVCAR-3	<10.0		4.1	2.2
OVCAR-4	30.9	17.0	56.2	39.3
OVCAR-5	1288.2	12.0	44.7	41.5
OVCAR-8	<10.0	11.2	>100.0	12.4
NCI/ADR-RES	<10.0	10.7	>100.0	12.7
SK-OV-3	<10.0	5.6	30.9	1.3
Renal cancer				
786–0	<10.0	2.0	9.1	-56.0
ACHN	<10.0	3.0	21.4	2.8
CAKI-1	<10.0	11.2	38.9	29.7
SN12C	<10.0	10.0	45.7	30.9
TK-10	1122.0	7.9	49.0	10.7
UO-31	<10.0	3.0	35.5	13.6
Prostate Cancer				
PC-3	<10.0	4.8	34.7	-0.9
DU-145	<10.0	11.5	38.0	18.2
Breast cancer				
MCF7	56.2	2.9	49.0	2.1
MDA-MB-231	<10.0	1.9	30.2	-20.3
HS 578T	<10.0	10.2	>100.0	31.1
BT-549	<10.0	2.7	10.5	18.4
T-47D	1258.9	4.4	53.7	30.5
MDA-MB-468	17.8	1.5	6.9	-36.7

Supplement Table 4. Assay and reference compound for safety screen data

	ASSAY	REFERENCE COMPOUND
specific binding assay	A2A (h) (agonist radioligand)	NECA
	alpha 1A (h) (antagonist radioligand)	WB 4101
	alpha 2A (h) (antagonist radioligand)	yohimbine
	beta 1 (h) (agonist radioligand)	atenolol
	beta 2 (h) (agonist radioligand)	ICI 118551
	BZD (central) (agonist radioligand)	diazepam
	CB1 (h) (agonist radioligand)	CP 55940
	CB2 (h) (agonist radioligand)	WIN 55212-2
	CCK1 (CCKA) (h) (agonist radioligand)	CCK-8s
	D1 (h) (antagonist radioligand)	SCH 23390
	D2S (h) (agonist radioligand)	7-OH-DPAT
	ETA (h) (agonist radioligand)	endothelin-1
	NMDA (antagonist radioligand)	CGS 19755
	H1 (h) (antagonist radioligand)	pyrilamine
	H2 (h) (antagonist radioligand)	cimetidine
	MAO-A (antagonist radioligand)	clorgyline
	M1 (h) (antagonist radioligand)	pirenzepine
	M2 (h) (antagonist radioligand)	methoctramine
	M3 (h) (antagonist radioligand)	4-DAMP
	alpha 4beta 2 (h) (agonist radioligand)	nicotine
	delta 2 (DOP) (h) (agonist radioligand)	DPDPE
	kappa (KOP) (agonist radioligand)	U 50488
	mu (MOP) (h) (agonist radioligand)	DAMGO
	5-HT1A (h) (agonist radioligand)	8-OH-DPAT
	5-HT1B (antagonist radioligand)	serotonin
	5-HT2A (h) (agonist radioligand)	(±)DOI
	5-HT2B (h) (agonist radioligand)	(±)DOI
	5-HT3 (h) (antagonist radioligand)	MDL 72222
	GR (h) (agonist radioligand)	dexamethasone
	AR (h) (agonist radioligand)	mibolerone
	V1a (h) (agonist radioligand)	[d(CH2)51,Tyr(Me)2]-AVP
	Ca2+ channel (L, dihydropyridine site) (antagonist radioligand)	nitrendipine
	KV channel (antagonist radioligand)	alpha -dendrotoxin
	Na+ channel (site 2) (antagonist radioligand)	veratridine
	NE transporter (h) (antagonist radioligand)	protriptyline
	DA transporter (h) (antagonist radioligand)	BTCP
	5-HT transporter (h) (antagonist radioligand)	imipramine
enzyme-based assay	COX1 (h)	diclofenac
	COX2 (h)	NS 398
	PDE3A (h)	milrinone
	PDE4D2 (h)	rolipram
	Lck kinase (h)	staurosporine
	acetylcholinesterase (h)	neostigmine

Supplement Figure 1. Western blot showing the elevated protein concentrations for each of the drug-selected and gene-transfected cell lines over-expressing ABCB1, ABCC1, and ABCG2. Primary antibodies against ABCB1 (#P7965, Sigma-Aldrich, St. Louis, MO), ABCC1 (#72202, Cell Signaling Technology, Danvers, MA), ABCG2 (#MAB4146, Sigma-Aldrich, St. Louis, MO) and GAPDH (#MA5-15738, Thermo Fisher Scientific, Rockford, IL) were used. HRP-linked secondary antibodies used were anti-mouse IgG (#7076) and anti-rabbit IgG (#7074) from Cell Signaling Technology, Danvers, MA.

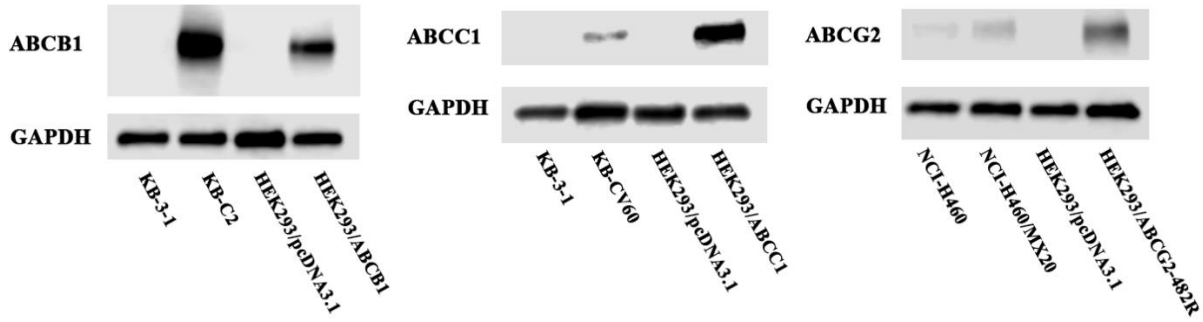

Supplement Figure 2. Effect of DJ95 on ABCB1 or ABCG2 vanadate-sensitive ATPase activity. (A) ABCB1-mediated ATP hydrolysis in the presence of DJ95 or positive substrate paclitaxel (0-10,000 nM). (B) ABCG2-mediated ATP hydrolysis in the presence of DJ95 or positive substrate topotecan (0-10,000 nM). Data are plotted with mean and error bars depict SD obtained from three independent experiments.

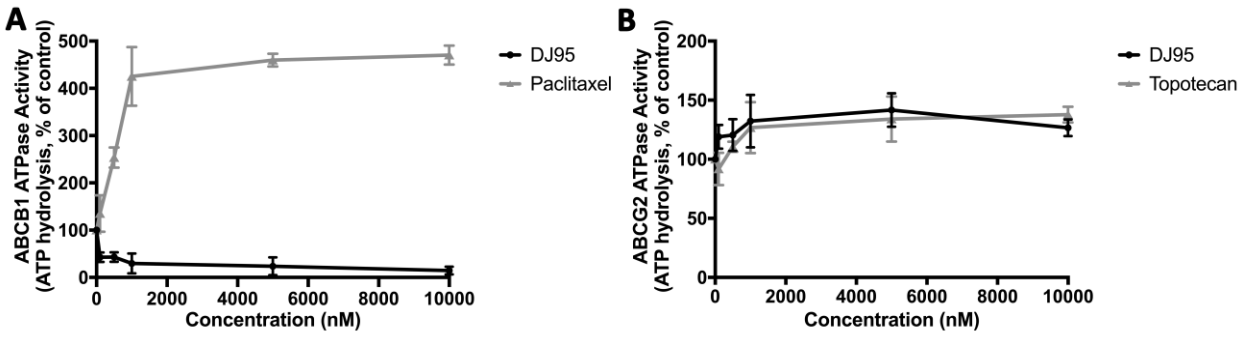

Supplement Figure 3. NCI-60 data for DJ95**.** (A) Sensitivity of NCI cancer cell lines to DJ95. 10 µM of DJ95 was used against cell lines to compare the growth percentage of each cell line relative to the no-drug control, and relative to the time zero number of cells. The percentage growth is represented by the horizontal bar, showing both growth inhibition (values between 0 and 100) and lethality (< 0). (B) Average growth percentage for each cancer type represented as mean ± SEM. (C) Dose-response curves for DJ95 against melanoma cancer cell lines.

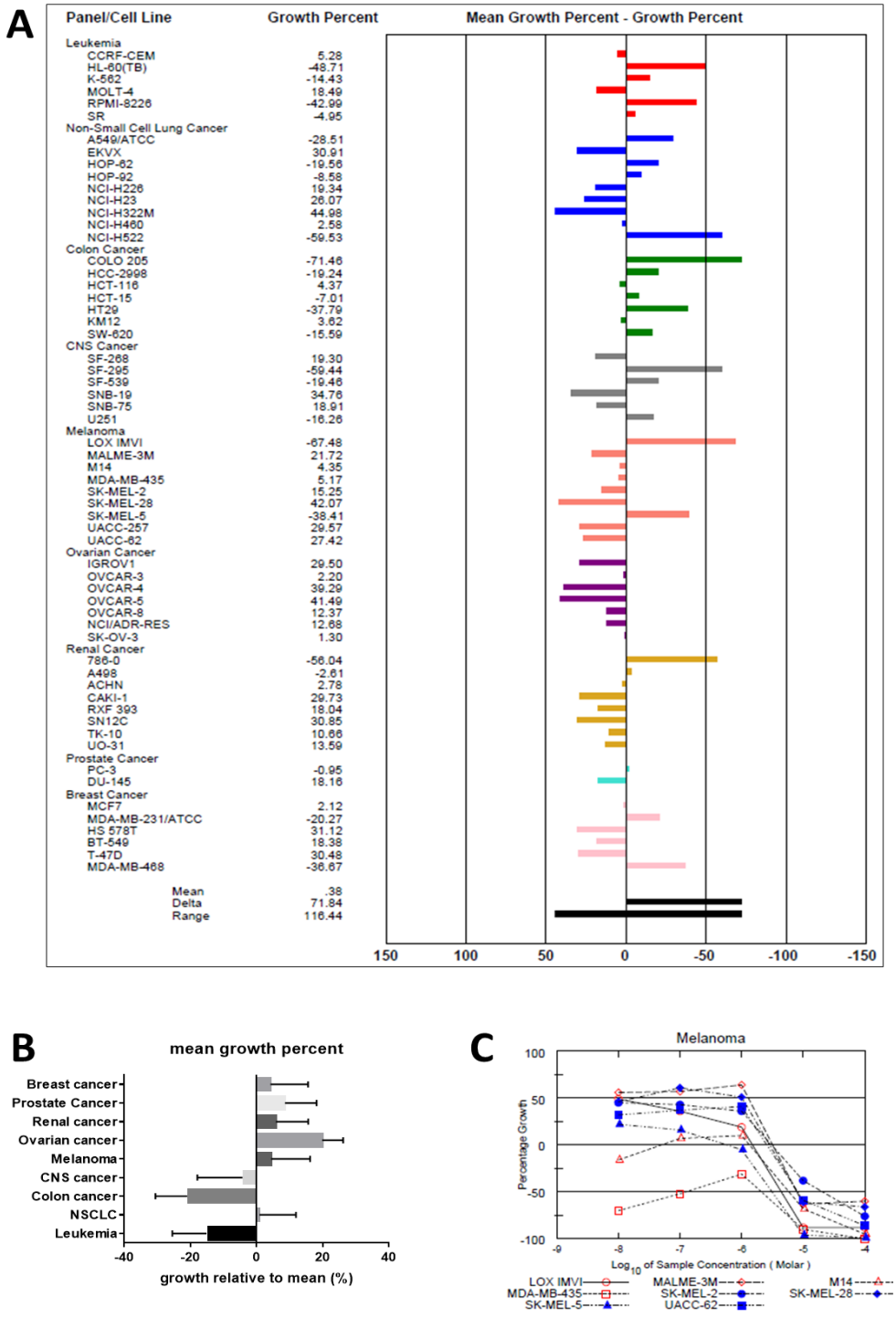

Supplement Figure 4. Scratch assay quantification. A375 and RPMI-7951 migration represented as total area in scratch channel ± SD. Statistical significance was determined by two-way ANOVA followed by Dunnett's multiple comparison test, comparing each treatment group to the control group at that specific time point. There was no significant difference for the area at time zero for any group. (*p< 0.05, ****p< 0.0001).

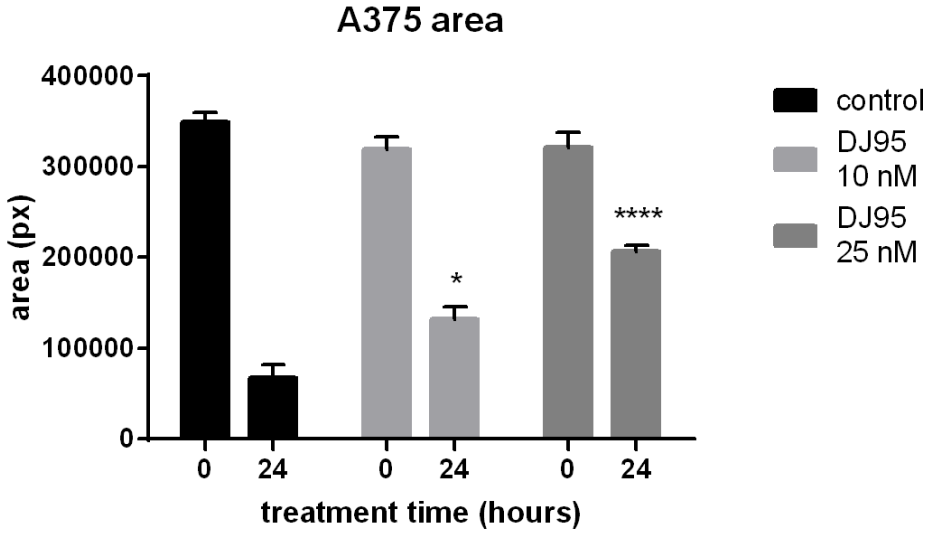

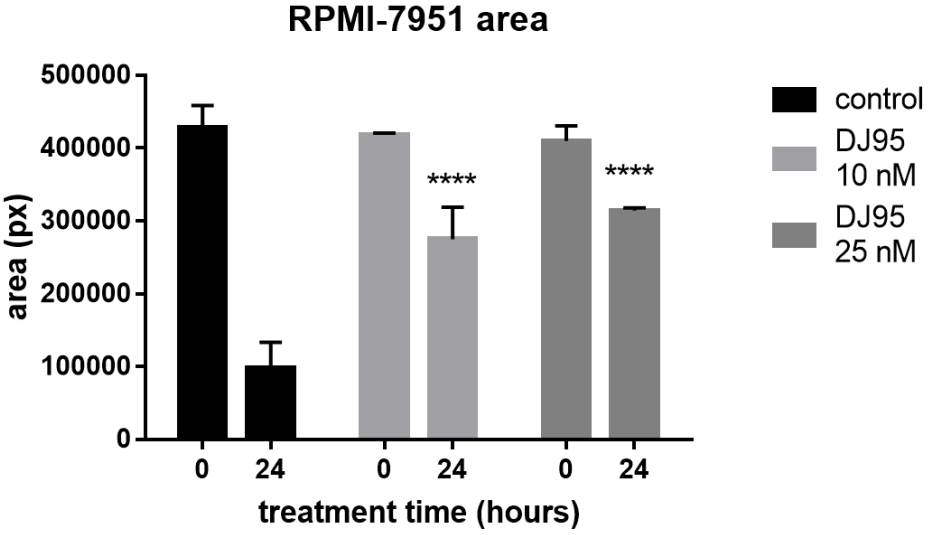

Supplement Figure 5. Electron density maps for DJ95. (A) 2Fo-Fc map contoured at 1 sigma. (B) Simulated annealing omit map contoured at 3 sigma.

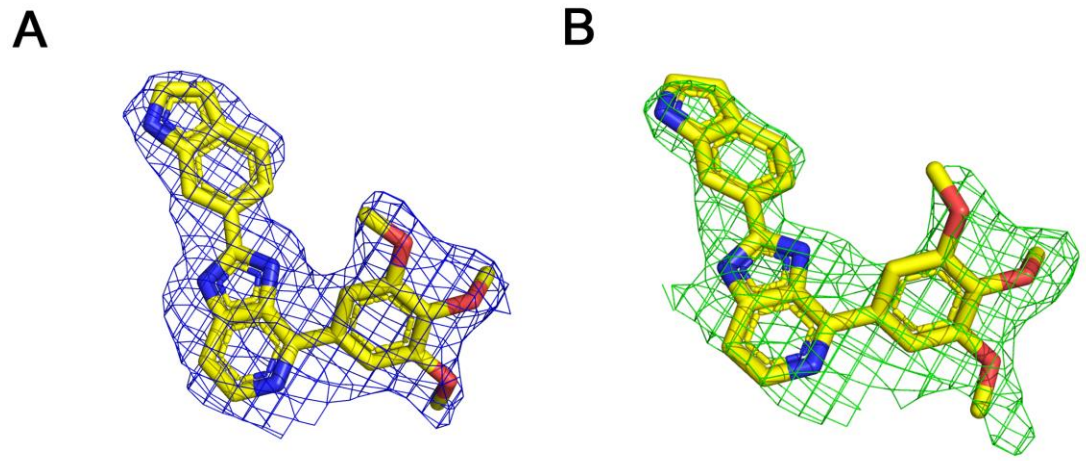

Supplement Figure 6. Images obtained from immunohistochemistry CD31 stained tumor sections at 20x magnification used for quantification of positive stained area for (A) control group and (B) DJ95 treated group. Five images were obtained from 3 separate tumors per group. Each row represents a separate tumor. Necrotic tissue area was avoided.